



In situ production of hybrid N₂O in dust-rich Antarctic ice

Lison Soussaintjean¹, Jochen Schmitt¹, Joël Savarino², J. Andy Menking^{3,4}, Edward J. Brook⁵, Barbara Seth¹, Vladimir Lipenkov⁶, Thomas Röckmann⁷, Hubertus Fischer¹

5

¹Climate and Environmental Physics, Physics Institute and Oeschger Centre for Climate Change Research, University of Bern, Bern, 3012, Switzerland

²University Grenoble Alpes, CNRS, IRD, Grenoble INP, INRAE, IGE, Grenoble, 38000, France

10 ³Australian Antarctic Program Partnership, Institute for Marine and Antarctic Studies, University of Tasmania, Hobart, Australia

⁴Environmental Research Unit Commonwealth Scientific and Industrial Research Organisation Aspendale, Victoria, Australia

⁵College of Earth, Ocean, and Atmospheric Sciences, Oregon State University, Corvallis, OR 97331, USA

⁶Climate and Environmental Research Laboratory, Arctic and Antarctic Research Institute, Saint Petersburg, 199397, Russia

15 ⁷Institute for Marine and Atmospheric research Utrecht (IMAU), Utrecht University, 3584CC Utrecht, the Netherlands

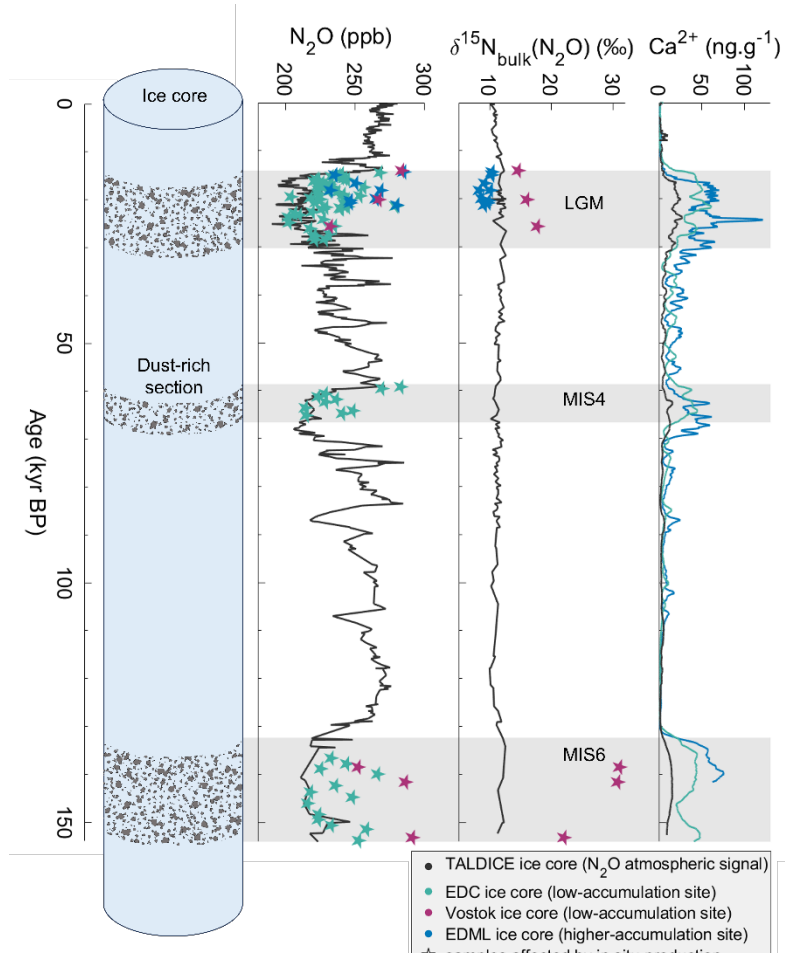
Correspondence to: Lison Soussaintjean (lison.soussaintjean@unibe.ch)

Abstract. Nitrous oxide (N₂O) is a potent greenhouse gas involved in the destruction of stratospheric ozone. Past atmospheric mixing ratios of N₂O are archived in ice cores; however, the presence of in situ N₂O production in dust-rich Antarctic ice complicates their accurate reconstruction, especially during glacial periods. This production occurs in 20 extremely cold ice and without sunlight. This study aims to understand the reaction producing N₂O in Antarctic ice by identifying the precursors and the reaction pathway. We compared the oxygen and nitrogen bulk and position-specific isotope composition of in situ N₂O in ice cores to the isotopic composition of nitrate (NO₃⁻), a possible precursor of N₂O. The ¹⁵N signature of NO₃⁻ is fully transferred into the central N atom (N_α) of in situ N₂O, but it is not transferred into the 25 terminal N atom (N_β), resulting in a 50 % transfer of the ¹⁵N signature of NO₃⁻ into the bulk ¹⁵N isotopic composition. These findings suggest that the in situ N₂O production involves two different nitrogen precursors present in ice: the central N atom (N_α) originates from NO₃⁻ and the terminal N atom (N_β) from a different precursor not yet identified. Oxygen isotope analysis shows that NO₃⁻ cannot be the only reservoir for the O atom of in situ N₂O. Temperature, pH, and absence of 30 sunlight in Antarctic ice point to an abiotic N-nitrosation reaction. The limiting factor of the reaction is probably associated with mineral dust and might be Fe²⁺, reducing NO₃⁻ to NO₂⁻ or the precursor of the N_β atom. The site preference (SP) values of in situ N₂O are highly variable between different ice cores and depend on the bulk ¹⁵N isotopic composition of N₂O, itself depending on the ¹⁵N isotopic composition of the NO₃⁻ precursor. This finding is unexpected because SP is usually determined by the production pathway through symmetric reaction intermediates that mix the N atoms in α and β positions and average out their isotopic difference. In contrast, our results provide the first evidence of a hybrid N₂O production pathway involving an asymmetric intermediate that preserves the distinct ¹⁵N signatures of two different precursors – one



35 contributing to the N_α atom and the other to the N_β atom. This finding has important implications: in this pathway, SP reflects the isotopic difference between the two precursors rather than the pathway itself, challenging how SP is commonly interpreted in environmental studies.

1 Introduction



40

45

Figure 1. N_2O mixing ratio, N_2O bulk nitrogen isotopic composition, and Ca^{2+} concentrations that represent the mineral dust content, measured in the TALDICE (Schilt et al., 2010a), EDC (Schilt et al., 2010b), EDML (Fischer et al., 2019), and Vostok (Miteva et al., 2007) ice cores. Because of its low dust content, the TALDICE record in black is considered to represent the true atmospheric N_2O levels (see Sect. 3.2.2). Stars correspond to samples affected by in situ production and represent the total N_2O measured, i.e., atmospheric N_2O + in situ N_2O . Grey boxes mark the dust-rich sections of the EDC ice core corresponding to the Last Glacial Maximum (LGM), the Marine Isotope Stage (MIS) 4 and 6 cold periods.



Nitrous oxide (N_2O) is a potent greenhouse gas whose global warming potential is 273 times higher than that of carbon dioxide (CO_2) on a 100-year timescale (IPCC, 2021). As a result of the anthropogenic alteration of the nitrogen cycle 50 (Gruber and Galloway, 2008), the N_2O atmospheric mixing ratio has risen by 23 % compared to pre-industrial levels (Rubino et al., 2019), reaching 338 ppb in December 2024 (Lan et al., 2025) and contributing around 6 % to the radiative forcing from long-lived greenhouse gases. N_2O is also the primary source of stratospheric nitrogen oxides (NO_x) that destroy ozone (Ravishankara et al., 2009).

Soils and aquatic environments are the main sources of atmospheric N_2O . Production of N_2O occurs both during 55 denitrification, the reduction of nitrate (NO_3^-) to nitrite (NO_2^-) and ultimately molecular nitrogen (N_2), and as a by-product of nitrification, where ammonium (NH_4^+) is oxidized to hydroxylamine (NH_2OH) and then converted to NO_2^- and NO_3^- (Baggs, 2011; Bange, 2008). N_2O is also produced during the reduction of NO_2^- to N_2O in nitrifier denitrification, where nitrifying microorganisms reduce NO_2^- to N_2O similarly to heterotrophic denitrifiers (Wrage-Mönnig et al., 2018). These reactions are 60 performed by bacteria, archaea and fungi, but abiotic reactions have also been documented (Zhu-Barker et al., 2015). These include chemo-denitrification (Jones et al., 2015; Tischer et al., 2022), which is the reduction of NO_3^- or NO_2^- by Fe(II), and NH_2OH oxidation by Fe(III) or Mn(IV).

The composition of the atmosphere in the past can be reconstructed by analyzing air trapped in polar and high-altitude ice cores. Ice cores are the only direct atmospheric archive and have provided continuous CO_2 and CH_4 records over the last 800,000 years covering eight glacial-interglacial cycles (Louergue et al., 2008; Lüthi et al., 2008) and a partial record of 65 N_2O . In addition to N_2O mixing ratios, measurement of the stable isotopic composition of N_2O is used for source attribution of N_2O emissions. In the current state of the climate system, natural sources account for 57 % of total N_2O emissions, while anthropogenic sources contribute the remaining 43 % (Tian et al., 2020). Natural sources are approximately 58 % emissions from soils, 38 % from marine ecosystems, and the remaining 4 % from lightning and atmospheric production (Tian et al., 2020). N_2O emissions from both land and marine ecosystems may have varied in the past. Because sources differ in their 70 isotopic signatures, past changes in terrestrial and marine emissions can be reconstructed using the isotopic composition of N_2O archived in ice cores (Fischer et al., 2019; Menking et al., 2020; Schilt et al., 2014). Furthermore, position-specific nitrogen isotope analysis provides an additional constraint for distinguishing N_2O production pathways (Bernard et al., 2006; Menking et al., 2025; Prokopiou et al., 2017, 2018). This analysis consists of measuring $\delta^{15}\text{N}$ of the central-position N atom ($\delta^{15}\text{N}_a$) and the terminal-position N atom ($\delta^{15}\text{N}_\beta$) in N_2O . The ^{15}N site preference ($\text{SP} = \delta^{15}\text{N}_a - \delta^{15}\text{N}_\beta$) is considered to be 75 independent of the $\delta^{15}\text{N}$ signature of the nitrogen precursor (Frame and Casciotti, 2010; Sutka et al., 2003, 2006; Toyoda et al., 2005).

However, the atmospheric signal of greenhouse gases archived in ice cores can be altered (Anklin et al., 1995; Delmas, 1993; Lee et al., 2020; Mühl et al., 2023). This is particularly true for N_2O : the N_2O mixing ratio in glacial period ice from Antarctica shows large scatter between nearby samples from the same core and different values between ice cores for the 80 same age (Fig.1) (Flückiger et al., 2002; Sowers, 2001; Stauffer et al., 2003), which is inconsistent with the homogeneous global atmospheric mixing ratio of N_2O resulting from its 123-year atmospheric lifetime (Prather et al., 2015) and the low-



pass filtering of the atmospheric signal through the slow bubble enclosure process. Because these anomalies were observed for ice core analyses using two distinct gas extraction methods – wet extraction by melting (Schilt et al., 2010b) and dry extraction by grating the ice (Sowers, 2001) – it was concluded that N_2O production occurred already in the ice sheet and not 85 during the analysis. This “*in situ* production” or excess N_2O in dust-rich sections of polar ice cores has two major consequences for the climatic interpretation. First, as the production process has not yet been identified, and the excess N_2O has not yet been quantified, we do not have access to past atmospheric N_2O mixing ratios during most past glacial periods 90 (Schilt et al., 2010b), where high dust contents are found in the ice. Secondly, samples affected by *in situ* production deviate from the isotopic composition of atmospheric N_2O (Fig.1), which precludes source attribution (Fischer et al., 2019; Schilt et al., 2014). It is therefore necessary to understand the N_2O production process(es) in the ice to systematically identify affected samples and thus avoid misinterpretation. Several detection methods were implemented to scrutinize the N_2O record (Flückiger et al., 2004; Spahni et al., 2005), but they were only used to discard the samples likely to be affected. Understanding the production processes could potentially provide a reliable way of quantifying the fraction of N_2O produced 100 *in situ* and to correct the measured signal with the aim to obtain the past atmospheric signal.

95 This work also has relevance for nitrogen cycle processes in extreme environments. Very few studies have focused on N_2O production under extreme conditions as those encountered in the Antarctic ice sheet, where temperatures reach down to -60 °C, pressures are enormous, and reaction time scales can be of the order of several thousand years. Priscu et al. (2008) measured very high N_2O mixing ratios in a permanently ice-covered lake in the Dry Valleys, Antarctica, which they attributed to microbial nitrification. Investigating N_2O production in Antarctic ice is an opportunity to explore whether 100 microorganisms can be metabolically active at -60 °C. Although previous studies suggested potential N_2O production by bacteria (Flückiger et al., 2002; Schilt et al., 2010b; Sowers, 2001), there is currently no evidence to support microbial activity in Antarctic ice as a source for *in situ* N_2O . High microbial counts have only been found in a few of the Vostok ice core samples where *in situ* production was reported (Sowers, 2001). Abiotic reactions may also cause N_2O formation in polar ice. In the Dry Valleys, Antarctica, Samarkin et al. (2010) demonstrated abiotic N_2O production by chemo-denitrification in 105 the Don Juan Pond soils.

This study uses isotope analysis to characterize *in situ* N_2O in ice. The background of the study and the extreme environmental conditions of the reactions involved are presented in Sect. 2. We measured the isotopic composition of N_2O in several ice cores and calculated the isotopic signature of *in situ* N_2O (Sect. 3 and 4). The isotopic composition of NO_3^- was also measured to identify potential precursors for the produced N_2O . Position-specific nitrogen isotope analysis of N_2O was 110 carried out to take a closer look into the reaction pathway(s). We discuss the potential reactions for *in situ* production of N_2O in Sect. 5.



2 Background – Potential precursors and reaction rate of N₂O production in polar ice

For both Greenland and Antarctic ice cores, N₂O production is inferred in ice-core sections corresponding to glacial periods, while there is no in situ production apparent for the Holocene and other interglacial and interstadial periods (Flückiger et al.,

115 Schilt et al., 2010b). The chemical composition of the ice differs significantly between glacial and interglacial periods, particularly in terms of its dust content. Dust concentrations are significantly higher during glacial periods than during interglacial periods (factor of 30-100) in Antarctic and Greenland ice cores (Fuhrer et al., 1999; Lambert et al., 2012). In fact, N₂O excess production is only observed in dust-rich ice and, in Antarctica specifically, it increases with higher dust concentrations (Fig. 1). This points to a reaction involving at least one compound contained in or associated with the dust.

120 The excess N₂O produced in Antarctic ice is on average 0.4 nmol N.kg⁻¹. The main nitrogen compounds that are generally considered as N₂O precursors are NO₃⁻ and NH₄⁺. The typical concentrations of NO₃⁻ and NH₄⁺ in ice are above 320 nmol N.kg⁻¹ and 55 nmol N.kg⁻¹, respectively (Kaufmann et al., 2010; Röthlisberger et al., 2000), and therefore more than sufficient to produce the observed excess N₂O. However, neither NO₃⁻ nor NH₄⁺ spontaneously react to N₂O. These precursors need to be activated by a chemical or biochemical agent, such as iron II (Fe²⁺) (Zhu-Barker et al., 2015) or 125 bacteria, respectively. Both Fe²⁺ (Spolaor et al., 2012, 2013) and bacteria (Miteva et al., 2016; Rohde et al., 2008; Sowers, 2001) were detected in polar ice.

Previous research has shown that samples affected by in situ production exhibit isotopic deviations from the atmospheric signature that differ in both direction and magnitude across ice cores (Fischer et al., 2019; Menking et al., 2025; Schilt et al., 2014; Sowers, 2001). It has been observed that the ¹⁵N signatures of total N₂O – i.e. atmospheric plus in situ N₂O – depend

130 on snow accumulation: sites with low accumulation show enrichment in ¹⁵N compared to the atmospheric signature (Sowers, 2001), while sites with higher accumulation show depletion in ¹⁵N (Fischer et al., 2019) (Fig. 1). A similar dependence of isotopic composition on accumulation rate is observed for NO₃⁻. The accepted reason is that after deposition some of the NO₃⁻ undergoes photolysis in the photic zone, corresponding to ca. the first meter of the surface snow. Kinetic isotope effects for photolysis favor the loss of the lighter isotopologues (i.e. containing ¹⁴N), resulting in ¹⁵N enrichment of the 135 remaining NO₃⁻ (Blunier et al., 2005; Frey et al., 2009). The fraction of photolyzed NO₃⁻ and the degree of isotopic enrichment depends on the time NO₃⁻ spends in the photic zone before it is archived in the ice by progressive burial. At low-accumulation sites, the duration within the photic zone is longer and a large fraction of NO₃⁻ is photolyzed leading to a highly ¹⁵N-enriched NO₃⁻ archived in the ice, reaching values of $\delta^{15}\text{N}_{\text{bulk}} = 300 \text{ ‰}$ at Concordia (Erbland, 2011; Erbland et al., 2013).

140 In ice core samples affected by in situ N₂O production, the presence of high $\delta^{15}\text{N}_{\text{bulk}}$ values of N₂O along with ¹⁵N-enriched NO₃⁻ strongly suggests that in situ N₂O production uses N from NO₃⁻. The isotopic composition of NH₄⁺ has never been measured in Antarctic ice cores, because large amounts of ice are required at the low NH₄⁺ concentrations, and the samples are highly sensitive to NH₃ contamination (Lamothe et al., 2023). Although a low contamination protocol has been developed by Lamothe et al. (2023), it was used for samples with higher NH₄⁺ concentrations, where the blanks are



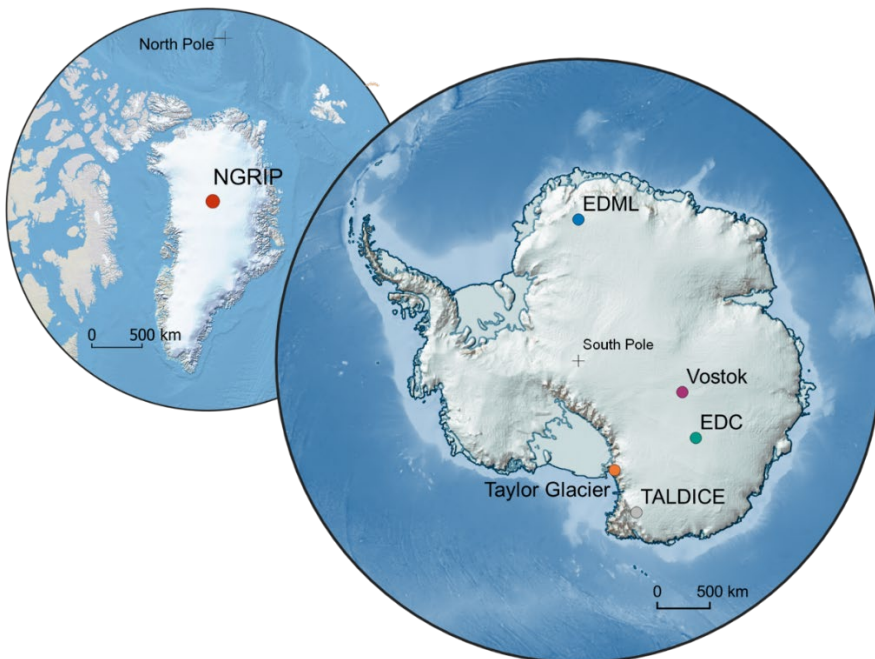
small compared to the sample concentration. Nonetheless, the hypothesis of NH_4^+ as an N_2O precursor is discussed in Sect.

145 5.1.

Regarding the reaction rate, the production of N_2O might already start near the surface of the ice sheet, in the snow and firn, but most of the produced N_2O would be lost to the atmosphere via air exchange. In the diffusive zone of the firn column and below the air lock-in depth (Battle et al., 1996), exchange of the firn air with the atmosphere is limited or excluded and the produced N_2O is partly or fully preserved in the ice. To be able to observe in situ N_2O in ice cores, the production must 150 continue close to or below the lock-in depth (located between 50 to 100 m, depending on the location and conditions of the ice sheet). For example, during the LGM at Vostok, Antarctica, the lock-in depth was around 94 m, and the age of the ice at this depth was 5200 years (Table 1). This means that at Vostok, N_2O was still produced several thousand years after the precursors were deposited onto the ice sheet. This observation shows that either it takes time for the precursors to come into contact, for example by diffusion in the ice, or that the reaction is very slow due to low temperatures. In the latter case, it 155 would not be possible to reproduce such slow reaction kinetics in the laboratory. This observation also shows that the reaction does not need light.

3 Samples and Methods

3.1 Ice core samples



160 **Figure 2. Location of the ice core drilling sites presented in this study. Maps created using the Quantarctica (Matsuoka et al., 2018) and QGreenland (Moon et al., 2023) QGIS data packages.**



To gain a comprehensive understanding of the N_2O production process(es) in diverse environmental settings, we analyzed 165 ice core samples from different sites with different characteristics: variable dust contents, variable dust chemical compositions, variable snow accumulation rates and therefore isotopic signatures of NO_3^- , and variable drilling site temperatures. These characteristics are reported in Table 1. Calcium (Ca^{2+}) concentrations are used as a proxy for dust content because they have been found to be correlated with mineral dust concentrations (Ruth et al., 2002). Figure 2 shows the location of the drilling sites.

We analyzed samples from five Antarctic ice cores: the Talos Dome Ice Core (TALDICE), the European Project for Ice 170 Coring in Antarctica (EPICA) Dome C core (EDC), the EPICA Dronning Maud Land core (EDML), the Vostok ice core, and the main transect of the Taylor Glacier (TG) blue ice area. Additionally, we analyzed samples from one Greenland ice core, the North Greenland Ice Core Project ice core (NGRIP). The TALDICE ice core was selected for its low dust content 175 (and suspected low degree of in situ N_2O) compared to other Antarctic ice cores, the EDC and Vostok ice cores for their low snow accumulation rate, the EDML ice core for its relatively higher snow accumulation rate. The NGRIP ice core was analyzed to compare the isotopic signature of in situ N_2O in Greenland and Antarctic ice. The five latter ice cores were obtained from deep drilling and are stratigraphically ordered, with recent layers at the surface of the ice sheet and older 180 layers towards the bedrock. In contrast, the TG blue ice area exposes old ice – flowing from the Taylor Dome – at the surface due to local ice dynamics and ablation (Baggenstos et al., 2018). The TG ice core was sampled close to the surface along a transect where the horizontal stratigraphy is preserved, a so-called “horizontal core.” The age of the ice then varies with distance along this transect.

We measured the stable isotopic composition ($\delta^{15}\text{N}_{\text{bulk}}$ and $\delta^{18}\text{O}$) of N_2O in the TALDICE, EDC, EDML, Vostok, TG and NGRIP ice cores, and the stable isotopic composition ($\delta^{15}\text{N}$ and $\delta^{18}\text{O}$) of NO_3^- in all samples except NGRIP. We also carried out position-specific isotope analysis of the central ($\delta^{15}\text{N}_{\alpha}$) and terminal ($\delta^{15}\text{N}_{\beta}$) nitrogen atoms in N_2O in the Vostok and TG ice cores.

185 The samples date from either the Last Glacial Maximum (LGM) and glacial-interglacial transition (14 to 29 ka), Marine Isotope Stage 4 (MIS4, 57 to 71 ka), or Marine Isotope Stage 6 (MIS6, 130 to 191 ka), which are all dust-rich glacial periods and are therefore prone to in situ production of N_2O . We selected samples younger than 150 ka because the N_2O atmospheric baseline recorded in the dust-poor TALDICE ice core and used in our mass balance approach (see Sect. 3.2.2) does not extend to older periods.

190 **Table 1. Characteristics of the ice core drilling sites presented in this study.**

	TG [†]	Vostok	EDC	EDML	TALDICE	NGRIP
Latitude (°)	-77.7598 ^b	-78.4642	-75.1000	-75.0019	-72.8302	75.1000
Longitude (°)	161.7212 ^b	106.8370	123.3326	0.0663	159.2004	-42.32
https://add.scar.org/						



Elevation (MSL) (https://add.scar.org/)	580	3488	3233	2892	2320 ^c	2917
accumulation rate^{*a} in ice equivalent per year (cm)	0.8 ^b	1.2	1.4	3.7	4.5	6.3
Age maximum^a (ka)	150	408	813	145	343 ^d	125
Annual mean snow surface temperature* (°C)	-46 ^f	-66 ^e	-60 ^e	-53 ^e	-44 ^e	-46 ^f
Maximum depth where the N₂O production occurred (m)	-	300	400	770	750	1600
Temperature range of the ice where the production occurred (bore hole temperature) (°C)	-	-56.6 - -55.2 ^g	-53.6 - -51.6 ^h	~ -40 ⁱ	-	-30 - -32 ^j
Ice age – Gas age difference (Δage)^{*a} (yr)	3350 ^b	5170	3960	1590	1000	890
Air lock-in depth^a (m)	29 ^f	94	83	84	70	79
Ca²⁺ concentration* (ng.g⁻¹)	21±15 ^b	-	35±21 ^k	47±37 ^l	16±9 ^m	292±187 ⁿ
Dominant source of dust	Southern South America (SSA) ^o	SSA ^p	SSA ^q	SSA ^q	SSA ^r	East Asian deserts ^s

^fspecial case: horizontal core. LGM mean snow surface temperature estimated based on δ¹⁸O(H₂O) data. LGM lock-in depth calculated using the Herron-Langway firn model with delta age and temperature inputs for the TG accumulation zone near Taylor Dome (Herron and Langway, 1980).

195 *averaged over the period 15 – 30 ka

^aBouchet et al. (2023)

^bBaggenstos et al. (2018)

^cBuiron et al. (2011)

^dCrotti et al. (2021)

200 ^eMarkle and Steig (2022)



^fKindler et al. (2014)

^gSalamatin et al. (1994)

^hRitz et al. (1982)

ⁱ[Wilhelms et al.](#) (2007)

205 ^jTarasov and Peltier (2003)

^kLambert et al. (2012)

^lFischer et al. (2007)

^mSchüpbach et al. (2014)

ⁿBigler (2024)

210 ^oAarons et al. (2017)

^pDelmonte et al. (2004)

^qMarino et al. (2009)

^rDelmonte et al. (2010)

^sRuth et al. (2003)

215 3.2 N₂O analysis

3.2.1 Measurement of N₂O mixing ratio and isotopic composition

Prior to analysis, the samples were decontaminated by removing ~5 mm of the outer surface potentially affected by diffusion of modern air and chemical contaminants. Scraping was performed with a precleaned knife and wearing polyethylene gloves to minimize NO₃⁻ contamination (see Sect. 3.3).

220 The mixing ratio and bulk isotopic composition of N₂O were measured at the University of Bern, Switzerland, using the method described in detail in Schmitt et al. (2014). The air was extracted by melting the ice core samples, N₂O was purified, analyzed by isotope ratio mass spectrometry (IRMS), and the results were converted to international isotope scales. Isotopic compositions are expressed in δ values where $\delta = \frac{R_{sample}}{R_{reference}} - 1$, with R referring to ¹⁵N/¹⁴N and ¹⁸O/¹⁶O ratios. The international references are N₂ in air for nitrogen and Vienna Standard Mean Ocean Water (VSMOW) for oxygen. The 225 analytical precision of N₂O mixing ratio, $\delta^{15}\text{N}_{\text{bulk}}$ and $\delta^{18}\text{O}$ values is 3 ppb, 0.3 ‰ and 0.4 ‰ respectively.

We analyzed the position-specific isotopic composition of N₂O from ice core samples at Oregon State University following gas extraction, IRMS analysis, and data reduction methods described in detail in Menking et al. (2025). The position-specific isotopic composition of N₂O, i.e. $\delta^{15}\text{N}_{\alpha}$ (central-position N atom), $\delta^{15}\text{N}_{\beta}$ (terminal-position N atom) and site preference (SP), is defined as:



$$\delta^{15}N_{bulk} = \frac{\delta^{15}N_\alpha + \delta^{15}N_\beta}{2} \quad (1)$$

$$SP = \delta^{15}N_\alpha - \delta^{15}N_\beta \quad (2)$$

The $\delta^{15}N_{bulk}$, $\delta^{15}N_\alpha$ and $\delta^{18}O$ values were measured and the $\delta^{15}N_\beta$ and SP values were calculated using Eq. (1) and (2), respectively. The precision of the measurement is 3 ppb for N_2O mixing ratio, $\pm 0.4\text{‰}$ for $\delta^{15}N_{bulk}$, $\pm 0.6\text{‰}$ for $\delta^{15}N_\alpha$, $\pm 0.8\text{‰}$ for $\delta^{15}N_\beta$, $\pm 1.3\text{‰}$ for SP , and $\pm 0.6\text{‰}$ for $\delta^{18}O$.

3.2.2 Calculation of the mixing ratio and bulk isotopic composition of the in situ N_2O fraction

The N_2O mixing ratio and isotopic composition that we measured represent the total N_2O extracted from the ice cores, i.e. a mixture of atmospheric N_2O plus any in situ N_2O . For our study, we need to calculate the mixing ratio and isotopic composition of in situ N_2O only. To calculate the in situ values from the measured values, we used the following mass balance approach for each sample:

$$[N_2O]_{in situ} = [N_2O]_{meas} - [N_2O]_{atm} \quad (3)$$

$$\delta_{in situ} = \frac{\delta_{meas} * [N_2O]_{meas} - \delta_{atm} * [N_2O]_{atm}}{[N_2O]_{in situ}} \quad (4)$$

where $[N_2O]_{meas}$ is the N_2O mixing ratio measured in the ice core sample, $[N_2O]_{in situ}$ is the mixing ratio of in situ N_2O in that sample, and $[N_2O]_{atm}$ is the atmospheric mixing ratio of N_2O at the gas age of the sample; the same terminology applies for delta values.

One issue with this mass balance approach is the need to know $[N_2O]_{atm}$ and δ_{atm} , given that most N_2O records are affected by in situ production. We used the N_2O record from the dust-poor TALDICE ice core, which is the best estimate of an atmospheric baseline. TALDICE is not significantly impacted by in situ N_2O production but is limited in time reconstruction (~150 ka). Low in situ contribution is supported by the observation that the TALDICE N_2O mixing ratios during the dust-rich LGM and MIS4 periods generally align with the NGRIP N_2O mixing ratios, after in situ N_2O outliers are removed from the NGRIP record (Fig. A1). Previous studies identified the high-resolution NGRIP record as representative of atmospheric N_2O variations (Flückiger et al., 2004; Schilt et al., 2010a, 2013). As atmospheric N_2O mixing ratios are globally homogeneous while in situ N_2O production is ice-core dependent, the agreement between the TALDICE and NGRIP records supports the atmospheric nature of the TALDICE record. This is particularly significant because the NGRIP and TALDICE ice cores, drilled in Greenland and Antarctica, respectively, have very different chemical compositions that would lead to different in situ production features. To associate each sample with the atmospheric values matching its gas age, we applied a cubic smoothing spline interpolation with a 2000-year smoothing window to the measured TALDICE data, which has a temporal resolution of approximately 300 years over the LGM and 600 years over MIS4. Only the samples with a mixing ratio difference of more than 15 ppb from the TALDICE spline were used in the mass balance calculation.

There are several sources of error in our approach, including measurement uncertainties in N_2O mixing ratios and isotopic composition, uncertainties in the TALDICE N_2O spline interpolation, and uncertainties in gas-age estimates, which in turn



impact the chronological alignment between ice cores. We used a Monte Carlo method to assess the uncertainty of reported values, and ran 1000 simulations to determine the mixing ratio and isotopic composition of in situ N_2O . We varied the 265 variables of Eq. (3) and (4) within their uncertainty ranges (Table B1). The derived uncertainties were calculated as the standard deviation of the results of the 1000 simulations.

We acknowledge that there could be a small in situ production of N_2O in the TALDICE ice core, isotopically undetectable if the isotopic signature of in situ N_2O is close to the atmospheric one. We conducted a sensitivity study to evaluate the impact of this possibility (Fig. C1 and C2). Assuming that N_2O production is proportional to dust content, we estimated the in situ 270 N_2O mixing ratios by multiplying the calcium concentrations – used as a dust proxy – by a constant N_2O production factor. These in situ N_2O mixing ratios were subtracted from the TALDICE N_2O mixing ratios to obtain a corrected record that was used in the mass balance approach as an atmospheric baseline. This approach assumes a constant total air content (TAC) across all samples. While variations in TAC affect the conversion from Ca^{2+} -based N_2O estimates (in ng.g^{-1}) to mixing ratios (ppb), this effect is relatively minor (within $\pm 10\%$) and does not dominate the overall uncertainty in our mass balance 275 calculation. Our sensitivity study varied the production factor from 0 to 1 ppb- $\text{N}_2\text{O}/\text{ng.g}^{-1}\text{-Ca}^{2+}$ (Fig. C1 and C2). A production factor above 0.5 ppb- $\text{N}_2\text{O}/\text{ng.g}^{-1}\text{-Ca}^{2+}$ is unlikely, as it would result in significantly lower N_2O mixing ratios in TALDICE compared to NGRIP. Increasing production factors in TALDICE result in isotopic signatures of in situ N_2O in the other ice cores that are closer to atmospheric values. Importantly, even with a small production factor of 0.1 to 0.2 ppb- $\text{N}_2\text{O}/\text{ng.g}^{-1}\text{-Ca}^{2+}$, our findings remain consistent, with minimal changes in regression slopes when comparing the isotopic 280 compositions of in situ N_2O and NO_3^- . Thus, we conclude that the interpretations that follow remain valid even if the assumption that TALDICE represents the true atmospheric N_2O baseline is not entirely accurate.

3.2.3 Calculation of the position-specific isotopic composition of the in situ N_2O fraction

We used the same mass balance approach as in Sect. 3.2.3 to calculate the in situ $\delta^{15}\text{N}_\alpha$ values in the Vostok and TG samples, with Eq. (3) and (4) in which the δ values are substituted with $\delta^{15}\text{N}_\alpha$. The in situ $\delta^{15}\text{N}_\beta$ values were calculated with 285 Eq. (1) ($\delta^{15}\text{N}_\beta \text{ in situ} = 2 \delta^{15}\text{N}_{\text{bulk in situ}} - \delta^{15}\text{N}_\alpha \text{ in situ}$) and in situ SP values with Eq. (2) ($\text{SP}_{\text{in situ}} = \delta^{15}\text{N}_\alpha \text{ in situ} - \delta^{15}\text{N}_\beta \text{ in situ}$). One problem with this approach is that the TALDICE record does not include position-specific information. As the atmospheric reference $\delta^{15}\text{N}_{\alpha \text{ atm}}$, we therefore used the average of the values measured by Menking et al. (2025) in samples from the TG ice core during the period 16 to 21 ka, as these values vary little over time during the last glacial period. These specific samples were shown to be unaffected by in situ production by comparison with TALDICE and NGRIP.

290 3.3 Measurement of NO_3^- concentration and isotopic composition

After wet extraction and dry extraction of N_2O at the University of Bern and Oregon State University, respectively, the meltwater and melted ice chips from ice-core samples were used for nitrate isotope analysis. To avoid any chemical reaction and hence production or consumption of NO_3^- , the collected samples were refrozen and stored at -25°C .

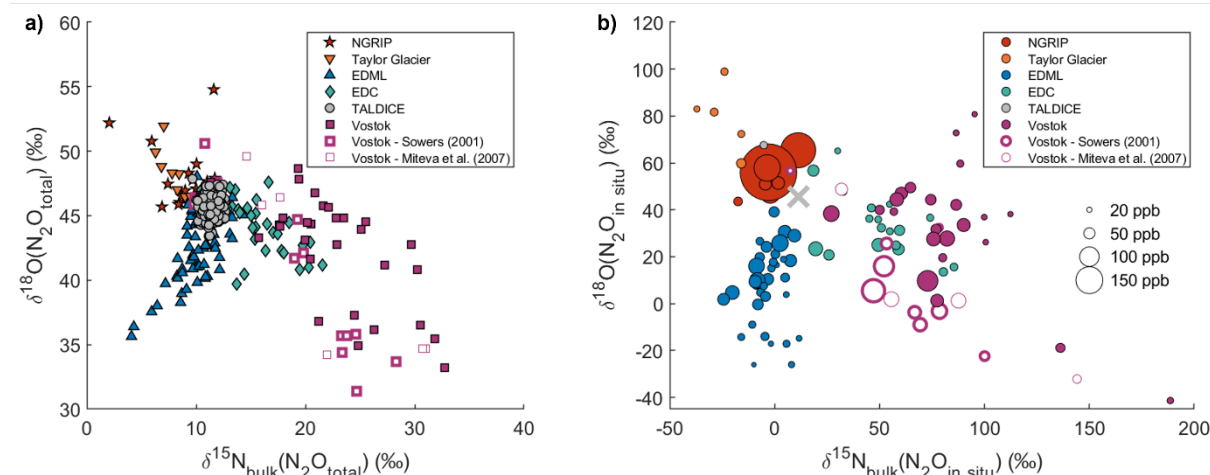


To assess the potential contamination impact of the gas extraction techniques on NO_3^- , we measured the concentration and 295 isotopic composition of NO_3^- in ultrapure ice samples spiked with a controlled amount of NO_3^- isotope standard after gas extraction as described above. Additionally, we compared the concentration and isotopic composition of NO_3^- in duplicate ice core samples, one analyzed directly and the other analyzed after gas extraction (Table D1). These tests show that the gas 300 extraction techniques do not lead to measurable contamination, loss, or $\delta^{15}\text{N}$ isotopic fractionation of NO_3^- in the collected samples. Although $\delta^{18}\text{O}(\text{NO}_3^-)$ values are slightly affected, the impact is negligible relative to their typical variability observed in ice cores.

The method used for nitrate isotope analysis is described in detail in previous publications (Erblund et al., 2013; Kaiser et al., 2007; Morin et al., 2009). Briefly, NO_3^- in the samples was preconcentrated using an ion exchange resin, then converted to N_2O through bacterial denitrification, using a strain of *Pseudomonas aureofaciens*. The resulting N_2O was then decomposed to N_2 and O_2 on a gold catalyst kept at 850 °C, and the isotopic compositions of the obtained N_2 and O_2 were measured by 305 IRMS. The results were corrected for blank contribution and calibrated on international scales following the procedure described in Erblund et al. (2013). Measurement errors are $\pm 0.8 \text{ ‰}$ for $\delta^{15}\text{N}$ and $\pm 1.0 \text{ ‰}$ for $\delta^{18}\text{O}$.

4 Results

4.1 Bulk isotopic signatures of total N_2O and in situ N_2O



310 **Figure 3. Nitrogen and oxygen isotopic composition of total N_2O measured in samples from different ice cores (a) and nitrogen and oxygen isotopic composition calculated for in situ N_2O in the same samples (b). The mixing ratio of in situ N_2O is represented by the size of the markers. The grey cross represents the average isotopic signature of the TALDICE samples and reflects the isotopic composition of atmospheric N_2O . In panel (b), one TALDICE sample shows in situ N_2O production associated with an exceptionally high dust peak (see Text). Note that the scale of the axes is different for panel (a) and (b).**



Figure 3a illustrates the measured isotopic signatures of total N_2O from various ice cores. The TALDICE data, representing atmospheric N_2O , clusters around a mean $\delta^{15}\text{N}_{\text{bulk}}$ value of $+11.3 \pm 0.7 \text{ ‰}$ (1σ standard deviation) and a mean $\delta^{18}\text{O}$ value of $+45.7 \pm 0.9 \text{ ‰}$. These data cover the last 140-kyr interval and their standard deviation is only about two times the measurement error, hence the detectable temporal variability of the isotopic signature of N_2O is small. In contrast, other ice
320 cores show wider ranges, both in $\delta^{15}\text{N}_{\text{bulk}}$ and $\delta^{18}\text{O}$: the deviations from the atmospheric range and relationship with elevated N_2O mixing ratios indicate that these samples are substantially affected by in situ production.

Importantly, the magnitude and direction of deviations from the atmospheric signature are ice core specific. Because the in
325 situ N_2O fraction shapes the observed isotopic deviations, we closely examine the isotopic signature of in situ N_2O in Fig. 3b, which presents the results of our mass balance calculation. Individual samples in the NGRIP ice core in Greenland show the highest in situ N_2O production, up to 380 ppb, while Antarctic ice cores like Vostok, EDML, EDC, and TG show in situ production in the order of 40 ppb, which corresponds to 20 % of the atmospheric N_2O mixing ratios during glacial periods. The isotopic signature of in situ N_2O is highly variable, ranging from -37 ‰ to $+189 \text{ ‰}$ for $\delta^{15}\text{N}_{\text{bulk}}$ and from -41 ‰ to $+100 \text{ ‰}$ for $\delta^{18}\text{O}$. Not only does in situ N_2O have a distinct isotopic signature in each ice core, it also exhibits a variable isotopic signature within a given ice core. This suggests that the isotopic signature of the precursor(s) varies. Interestingly, all the ice
330 cores except EDML show a negative correlation between $\delta^{15}\text{N}_{\text{bulk}}(\text{N}_2\text{O}_{\text{in situ}})$ and $\delta^{18}\text{O}(\text{N}_2\text{O}_{\text{in situ}})$ (Fig. 3b). EDML shows a positive correlation.

While we used the TALDICE N_2O record to represent atmospheric N_2O , it is important to note that one sample within this ice core record is affected by in situ production (Fig. 3b). By comparison with the TALDICE spline, this particular sample contains 31 ppb of in situ N_2O with a $\delta^{15}\text{N}_{\text{bulk}}(\text{N}_2\text{O}_{\text{in situ}})$ value of -5 ‰ and a $\delta^{18}\text{O}(\text{N}_2\text{O}_{\text{in situ}})$ value of $+67 \text{ ‰}$. Despite this
335 anomaly, there are compelling reasons to use TALDICE as a reliable record for atmospheric values. Firstly, only one sample out of the 192 measured was found to be affected by in situ production, indicating that such occurrences are rare. Indeed, this sample is characterized by an exceptionally high dust content of 188 ng.g^{-1} of Ca^{2+} , which is 280 % higher than typical dust peaks observed in the TALDICE ice core during the LGM. Secondly, the amount of in situ N_2O in the affected sample is relatively small compared to this high dust content: it corresponds to a production factor of 0.16 ppb of N_2O per ng.g^{-1} of
340 Ca^{2+} , which has little influence on our results, as shown by our sensitivity study (Fig. C2).

4.2 Comparison of isotopic compositions of NO_3^- and in situ N_2O

In this section, we compare the isotopic composition of NO_3^- and in situ N_2O to test our hypothesis that NO_3^- is a precursor for in-situ produced N_2O . We compare the isotopic composition of N_2O and NO_3^- measured in the same ice samples, with N_2O analyzed in the extracted air and NO_3^- in the meltwater collected after air extraction. To compare the data, we used the
345 regression method by York et al. (2004) that accounts for errors in both the x and y variables and their potential correlation.

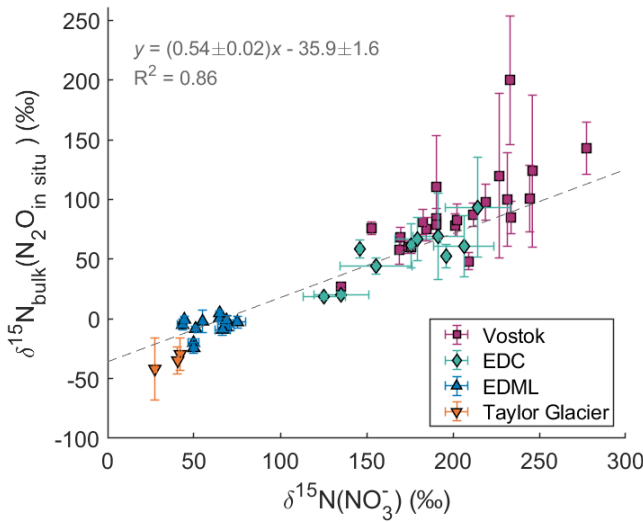


Figure 4. Relation between $\delta^{15}\text{N}_{\text{bulk}}(\text{N}_2\text{O}_{\text{in situ}})$ and $\delta^{15}\text{N}(\text{NO}_3^-)$. The dashed line represents the linear regression.

Figure 4 shows the bulk nitrogen isotopic composition of in situ N_2O and the nitrogen isotopic composition of NO_3^- measured in the EDML, EDC, TG and Vostok ice cores. There is a clear positive correlation between $\delta^{15}\text{N}_{\text{bulk}}(\text{N}_2\text{O}_{\text{in situ}})$ and $\delta^{15}\text{N}(\text{NO}_3^-)$ with a R^2 value of 0.86 which points to nitrate being a key precursor for the in situ produced N_2O . However, the slope is significantly different from 1, and in fact close to one half (0.54 ± 0.02), i.e., roughly one of the two N atoms of the in situ produced N_2O originates from NO_3^- .

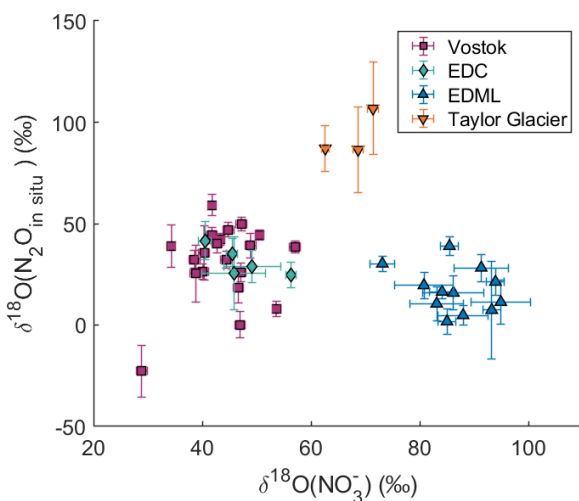


Figure 5. Relation between $\delta^{18}\text{O}(\text{N}_2\text{O}_{\text{in situ}})$ and $\delta^{18}\text{O}(\text{NO}_3^-)$.



Figure 5 shows the comparison between the $\delta^{18}\text{O}$ values of NO_3^- and in situ N_2O . There is no correlation between these two variables across or within sites, and no general trend towards ^{18}O enrichment or depletion of in situ N_2O relative to NO_3^- . At 360 Vostok and EDC, $\delta^{18}\text{O}(\text{NO}_3^-)$ values are around $+45 \pm 6 \text{ ‰}$ (1σ), while $\delta^{18}\text{O}(\text{N}_2\text{O}_{\text{in situ}})$ values are approximately $+31 \pm 17 \text{ ‰}$. At TG, $\delta^{18}\text{O}(\text{NO}_3^-)$ values are higher at $+68 \pm 4 \text{ ‰}$, and $\delta^{18}\text{O}(\text{N}_2\text{O}_{\text{in situ}})$ values reach $+93 \pm 11 \text{ ‰}$. At EDML, $\delta^{18}\text{O}(\text{NO}_3^-)$ values are the highest at $+87 \pm 6 \text{ ‰}$, whereas $\delta^{18}\text{O}(\text{N}_2\text{O}_{\text{in situ}})$ values are the lowest, at $+17 \pm 11 \text{ ‰}$.

In summary, despite the clear correlation between $\delta^{15}\text{N}_{\text{bulk}}(\text{N}_2\text{O}_{\text{in situ}})$ and $\delta^{15}\text{N}(\text{NO}_3^-)$ values suggesting NO_3^- as a precursor, the incomplete transfer of both its nitrogen and oxygen isotopic compositions to in situ N_2O indicates that NO_3^- alone does 365 not fully account for the nitrogen and oxygen sources of in situ N_2O . To gain deeper insights into the reaction mechanisms, we turn our focus to the position-specific isotopic composition of in situ N_2O .

4.3 Site preference of ^{15}N in in situ N_2O

Figure 6 shows clear correlations of $\delta^{15}\text{N}_a$, $\delta^{15}\text{N}_\beta$, and SP values versus $\delta^{15}\text{N}_{\text{bulk}}$ of total N_2O (a, c) and in-situ N_2O (b, d) measured in the TG and Vostok.

370

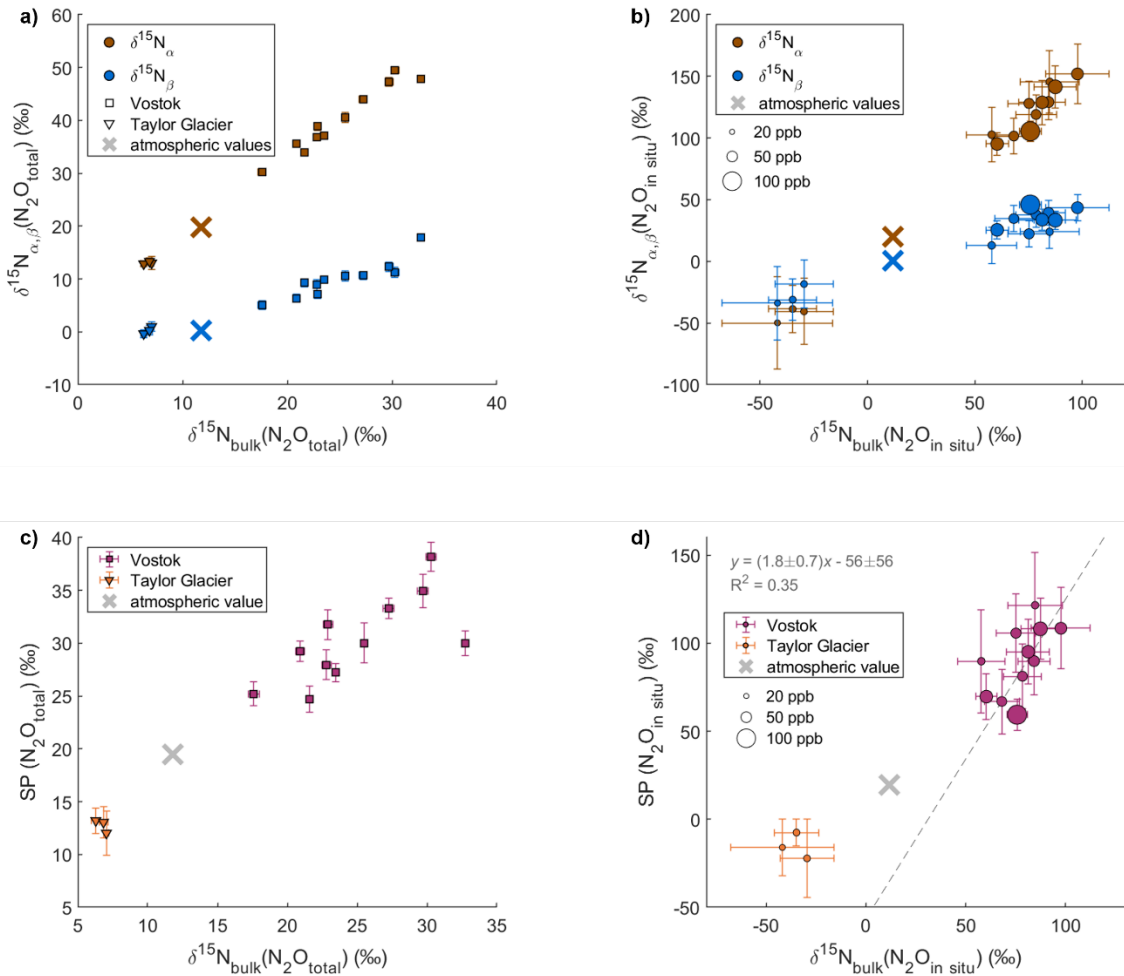
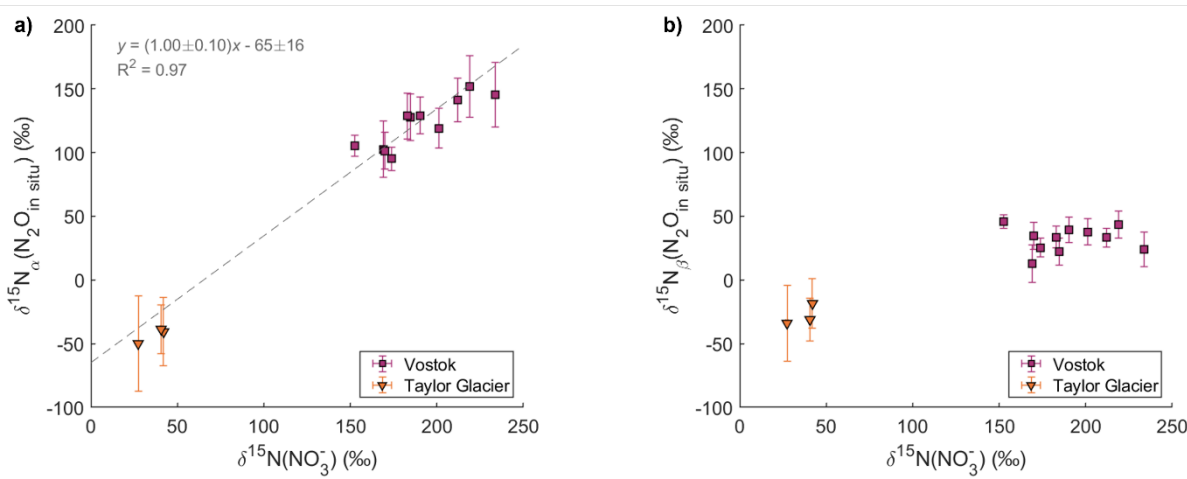


Figure 6. Position-specific isotopic composition measured for total (atmospheric + in situ) N_2O and calculated for in situ N_2O in the Vostok and TG ice cores. The panels show the relation between $\delta^{15}\text{N}_{\alpha}$, $\delta^{15}\text{N}_{\beta}$ and $\delta^{15}\text{N}_{\text{bulk}}$ of total N_2O (atmospheric + in situ) (a) and in situ N_2O (b), and between site preference (SP) and $\delta^{15}\text{N}_{\text{bulk}}$ of total N_2O (atmospheric + in situ) (c) and in situ N_2O (d). The size of the markers on panel (b) and (d) are scaled to the amount of in situ N_2O in the sample. In panel (b), TG samples are in the bottom-left corner. The crosses represent the unaffected atmospheric values measured by Menking et al. (2025) in dust-poor Taylor Glacier samples from the period 16 to 21 ka.

In situ N_2O at Vostok exhibits high $\delta^{15}\text{N}_{\alpha}$ values from +95 ‰ to +152 ‰ and much lower $\delta^{15}\text{N}_{\beta}$ values from +13 ‰ to +43 ‰. In contrast, in situ N_2O at TG has low $\delta^{15}\text{N}_{\alpha}$ values from -50 ‰ to -39 ‰ and low $\delta^{15}\text{N}_{\beta}$ values from -34 ‰ to -18 ‰, with $\delta^{15}\text{N}_{\alpha}$ being lower than the $\delta^{15}\text{N}_{\beta}$ values. The Vostok and TG samples exhibit very different $\text{SP}(\text{N}_2\text{O}_{\text{in situ}})$ values; +59 ‰ to +122 ‰ and -22 ‰ to -8 ‰, respectively. These values differ significantly from those of atmospheric N_2O which range in SP from +17 ‰ to +24 ‰ across last glacial termination, as reconstructed from dust-poor sections of TG ice (Menking et al., 2025). The $\text{SP}(\text{N}_2\text{O}_{\text{in situ}})$ values at Vostok are very high and variable, and are outside the range of typical reported values



385 from -11 ‰ to +37 ‰ (Toyoda et al., 2017; Zhu-Barker et al., 2015). Note that the $SP(N_2O_{in situ})$ values at Vostok seem to be correlated to the $\delta^{15}N_{bulk}(N_2O_{in situ})$ values with a slope of 1.8 ± 0.7 , whereas SP values in field and culture studies have been shown to be generally independent of $\delta^{15}N_{bulk}$ (Frame and Casciotti, 2010; Sutka et al., 2003, 2006; Toyoda et al., 2005). For TG, there is too little data to identify a potential correlation.



390 **Figure 7. Relation between $\delta^{15}N_\alpha(N_2O_{in situ})$ and $\delta^{15}N(NO_3^-)$ (a) and between $\delta^{15}N_\beta(N_2O_{in situ})$ and $\delta^{15}N(NO_3^-)$ (b).**

In Fig. 7, the $\delta^{15}N_\alpha$ and $\delta^{15}N_\beta$ values of in situ N_2O are compared with $\delta^{15}N$ values of NO_3^- measured in the TG and Vostok ice cores. There is a clear positive correlation between $\delta^{15}N_\alpha(N_2O_{in situ})$ and $\delta^{15}N(NO_3^-)$ with a slope of 1.0 ± 0.1 and an R^2 value of 0.97. This correlation is robust when excluding the TG data. However, there is no statistically significant correlation between $\delta^{15}N_\beta(N_2O_{in situ})$ and $\delta^{15}N(NO_3^-)$ for the individual sites.

5 Discussion

5.1 Production of hybrid N_2O

The strong correlation between $\delta^{15}N_{bulk}(N_2O_{in situ})$ and $\delta^{15}N(NO_3^-)$ indicates that NO_3^- is involved in the in situ N_2O formation. However, the slope is (0.54 ± 0.02) (Fig. 4), whereas a slope of 1 would be expected if both nitrogen atoms in N_2O originate from NO_3^- in the ice. Therefore, our results suggest that in situ N_2O is not derived from NO_3^- alone, thus not originate from a single precursor (we use the term “single-precursor N_2O ” hereafter, see Fig. 8). The strong correlation of $\delta^{15}N_\alpha(N_2O_{in situ})$ and $\delta^{15}N(NO_3^-)$ with a slope of 1.0 ± 0.1 (Fig. 7a), implies that the central N atom in N_2O (N_α), originates exclusively from NO_3^- archived in the ice. At the same time, the $\delta^{15}N_\beta(N_2O_{in situ})$ values are not correlated to $\delta^{15}N(NO_3^-)$, indicating that the terminal N atom (N_β) originates from a different nitrogen source. The slope of the linear regression between $SP(N_2O_{in situ})$ and $\delta^{15}N_{bulk}(N_2O_{in situ})$ (1.8 ± 0.7) is consistent, within uncertainty, with transfer of a variable N



isotopic composition from NO_3^- to N_α and transfer of a constant N isotopic composition from another precursor to N_β . Indeed, by substitution of equations Eq. (1) and (2), one would expect $\text{SP} = 2 * \delta^{15}\text{N}_{\text{bulk}} - 2 * \delta^{15}\text{N}_\beta$, where $\delta^{15}\text{N}_\beta$ is relatively constant within each ice core, although its specific value differs between cores (Fig. 7b). Our results suggest that the N_2O produced in situ is thus “hybrid N_2O ”, defined by its two nitrogen atoms originating from two distinct nitrogen precursors, one of them being NO_3^- in ice (Fig. 8).

410 A large number of studies have reported the production of hybrid N_2O through various reaction pathways, including N-nitrosation reactions (Spott et al., 2011) and the decomposition of ammonium nitrate (NH_4NO_3) (Rubasinghe et al., 2011). N-nitrosation reactions generally involve the replacement of a hydrogen atom on a nucleophilic precursor by a nitroso (-N=O) group (Spott et al., 2011). Production of N_2O occurs during N-nitrosation under acidic conditions, when the nitrosating agent nitrite (NO_2^-) reacts with the nucleophile hydroxylamine (NH_2OH) to form nitroxyl (HNO). Two HNO molecules then dimerize to produce nitrous oxide (N_2O) and water (Spott et al., 2011). This reaction can be abiotic or mediated by bacteria, archaea, or fungi. Other nucleophilic species can react with NO_2^- to produce N_2O , such as azide (N_3^-), ammonium (NH_4^+), hydrazine (N_2H_4), or salicylhydroxamic acid ($\text{C}_7\text{H}_7\text{NO}_3$) (Spott et al., 2011). In the case of in situ N_2O , the central nitrogen N_α may originate from NO_2^- after reduction of NO_3^- , and the terminal nitrogen N_β may come from one such nucleophilic precursor (Fig. 8). Our work does not yet allow us to identify the nucleophilic precursor for N_β , especially because the presence and concentration of most of the N-bearing compounds in ice have not yet been investigated.

415 Another pathway for hybrid N_2O production is the decomposition of ammonium nitrate (NH_4NO_3), either by thermal decomposition or by a light-initiated reaction involving the photoreduction of NO_3^- to NO_2 coupled with the oxidation of 420 NH_4^+ to NH_2 , which react with each other to produce N_2O (Rubasinghe et al., 2011). However, several arguments challenge the feasibility of the NH_4NO_3 decomposition in ice. Firstly, the ice environment lacks sufficient heat for thermal 425 decomposition, and light penetration is minimal within the deep firn and ice, raising questions about the availability of sufficient energy for these reactions. The high activation energy of the decomposition would make the reaction very slow at the ice temperature. Additionally, if N_2O were produced from NH_4NO_3 , the oxygen atom in N_2O would originate from NO_3^- 430 and inherit its isotopic composition, yet the $\delta^{18}\text{O}$ values of in situ N_2O do not correlate with those of NO_3^- (Fig. 5). Finally, NO_3^- and NH_4^+ are present in dust-poor polar ice as well, where no in situ N_2O production is observed, and similarly, there is not necessarily in situ N_2O production everywhere in dust-rich ice from Greenland despite sufficient NO_3^- and NH_4^+ . In our view, an N-nitrosation reaction is more likely than a NH_4NO_3 decomposition reaction for N_2O production in ice.

435 NH_4^+ could provide the terminal nitrogen (N_β) of in situ N_2O also in the case of N-nitrosation. The $\delta^{15}\text{N}$ values of NH_4^+ in the atmosphere range from -20 ‰ to +25 ‰ (Chen et al., 2022), rather similar to the $\delta^{15}\text{N}_\beta$ values of in situ N_2O in Vostok and TG with average $\delta^{15}\text{N}_\beta$ values of -27 ‰ and +24 ‰, respectively. These differences could be due to post-depositional processes altering the isotopic composition of NH_4^+ differently at different drilling sites. The nitrogen isotopic composition of NH_4^+ has been measured only in one alpine glacier ice core, with $\delta^{15}\text{N}$ values ranging from -15 ‰ to +5 ‰ for the years 2013-2017 (Lamothe et al., 2023). To further investigate this hypothesis, we suggest measuring the nitrogen isotopic



440 composition of NH_4^+ in Antarctic ice cores, specifically from Vostok and Taylor Glacier, to compare with the $\delta^{15}\text{N}_\beta$ values of in situ N_2O .

5.2 Limiting factor of the reaction

One key observation is that the elevated N_2O mixing ratios during glacial periods are of similar magnitude over the last 800 kyr in the EDC ice core with no increase with depth/age (Schilt et al., 2010b). This observation suggests that N_2O in situ 445 production does not increase further over time and is essentially finished at the LGM (20 to 26.5 ka). Therefore, we hypothesize a mechanism that is limited by the concentration or transport/diffusion of a reactant. The limiting factor cannot be NO_3^- as the concentrations remain high over time. Thus, it could be the precursor of the terminal N atom (N_β) or the agent reducing NO_3^- to NO_2^- .

Indeed, because N-nitrosation reactions typically involve NO_2^- rather than NO_3^- (Spott et al., 2011), a prior conversion of 450 NO_3^- to NO_2^- is required. While this step can be carried out by denitrifying organisms, the extremely low temperatures and acidic conditions in Antarctic ice make an abiotic process more likely (see Sect. 5.5). NO_3^- can be abiotically reduced to NO_2^- by redox-active metal ions such as Fe^{2+} or Mn^{2+} (Zhu-Barker et al., 2015). This hypothesis is supported by the presence of Fe^{2+} in ice cores (Spolaor et al., 2012, 2013). Baccolo et al. (2021) found decreasing Fe^{2+} concentrations with depth in the TALDICE core, and below 1500 m only Fe^{3+} is present in the form of jarosite ($\text{KFe}^{3+}_3(\text{SO}_4)_2(\text{OH})_6$), a mineral that forms 455 through the oxidation of aeolian dust under acidic conditions. These findings indicate that Fe^{2+} undergoes slow post-depositional oxidation in the ice. One possible explanation is that NO_3^- oxidizes dust-derived Fe^{2+} , which could explain the observed link between dust content and in situ N_2O production. In this scenario, Fe^{2+} is the limiting factor for N_2O production, as it is progressively consumed during the conversion from NO_3^- to NO_2^- .

5.3 Site preference constraints on the N_2O production mechanism

460 **Table 2.** Site preference (SP) ranges measured for different N_2O production pathways compared to site preference ranges calculated for in situ N_2O in the Vostok and TG ice cores.

	Reaction pathway	SP range (%)	Suspected intermediate species	Reference
Single-precursor N_2O	Bacterial denitrification	[-5.1 ; -0.5]		(Toyoda et al., 2017)
	Nitrifier denitrification	[-10.7 ; +0.1]		(Toyoda et al., 2017)
	Nitrification	[+28.9 ; +36.6]	Hyponitrite (-ONNO-)	(Toyoda et al., 2002, 2017)



	Fungal denitrification	[+21.9 ; +37.1]	Hyponitrite (-ONNO-) Iron-cis-hyponitrite-complex	(Toyoda et al., 2017)
	Abiotic NO_2^- reduction	[+10 ; +30.1]		(Jones et al., 2015; Toyoda et al., 2005)
	Abiotic NH_2OH oxidation	[+29.5 ; +34.1]	Hyponitrite (-ONNO-)	(Heil et al., 2015; Toyoda et al., 2005)
Hybrid N_2O	Abiotic oxidation of NH_2OH by NO_2^-	[+34 ; +35]		(Heil et al., 2014)
	In situ production at Vostok	[+57.2 ; +187.4]	Asymmetric intermediate (unknown)	This study
	In situ production at TG	[-17.3 ; -6.9]	Asymmetric intermediate (unknown)	This study

Since many reaction pathways have specific SP values, the SP signature is commonly used to attribute N_2O production pathway to a specific pathway. High SP values ranging from +22 ‰ to +37 ‰ are reported for nitrification, fungal

465 denitrification, and abiotic reactions such as NO_2^- reduction and NH_2OH oxidation (Table 3). Several studies suggested that the similarity of the SP signatures for these distinct formation pathways is attributable to a common intermediate species – hyponitrous acid HONNOH_{cis} . During decomposition, this intermediate preferentially breaks at the $^{14}\text{N}-\text{O}$ bond over the $^{15}\text{N}-\text{O}$ bond, enriching the central N atom (N_a) in ^{15}N and explaining high SP values (Fig. 8a). In contrast, bacterial and nitrifier denitrification produce N_2O with low SP values from -11 ‰ to 0 ‰, which are thought to derive from a different 470 intermediate. Modeling work suggested a trans-hyponitrous structure that decomposes preferentially into $^{15}\text{N}^{14}\text{NO}$ due to kinetic isotope effects, thus explaining the low SP values of these formation pathways (Fig. 8a). Overall, in these cases, SP values are therefore determined by the decomposition step of the last intermediate into N_2O and are independent of the $\delta^{15}\text{N}$ values of the precursor (Fig. 8).

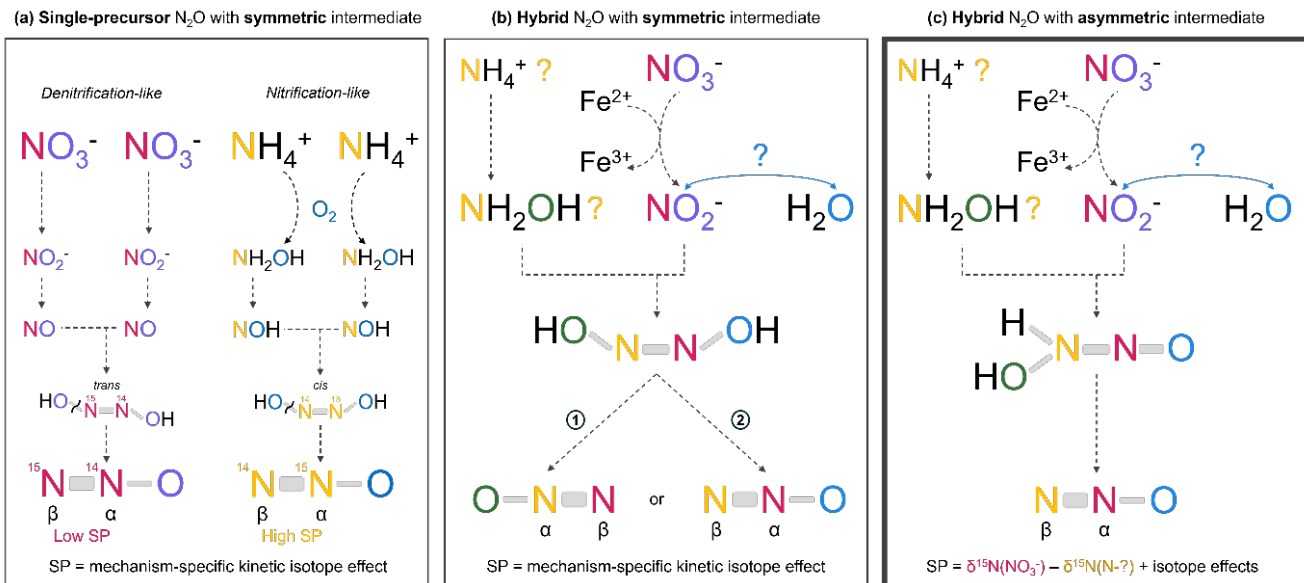
For in situ N_2O , however, the SP values for the Vostok and TG ice cores do not fall into either typical low or high SP range 475 and are highly variable (Table 2). The constant-SP pathways discussed above produce single-precursor N_2O , but in the case of hybrid N_2O production, one would expect a priori that the SP would no longer be a unique mechanism-dependent



signature. Instead, for hybrid reactions the SP should be influenced by the difference between the $\delta^{15}\text{N}$ signatures of the two precursors, if the central N atom (N_α) is derived from one precursor and the terminal N atom (N_β) from the other. However, Heil et al. (2014) demonstrated that hybrid N_2O from the nitrosation of NH_2OH by NO_2^- is also characterized by a constant 480 SP value of +34 ‰ (Table 2) regardless of the precursor signatures. The authors concluded that the NH_2OH -nitrosation mechanism also involves the symmetric hyponitrous intermediate (Fig. 8b). In fact, since this intermediate is symmetrical, the N atoms from each precursor can either take the α -position or the β -position in the final N_2O molecule; the difference in their $\delta^{15}\text{N}$ values then has no influence on the SP value (Fig. 8b).

Because of the variability of the $\text{SP}(\text{N}_2\text{O}_{\text{in situ}})$ values and their dependence on the $\delta^{15}\text{N}(\text{NO}_3^-)$ signature, we therefore deduce 485 that the production mechanism of in situ N_2O does not involve the hyponitrous symmetrical intermediate. In Fig. 8c, we propose a new reaction mechanism that involves an asymmetric intermediate, resulting in a hybrid N_2O molecule in which the N atoms at the α and β positions are derived from a specific precursor. N_α and N_β retain the two individual signatures of the precursors rather than losing them as discussed above. The high variability of SP values is then attributable to the variability of $\delta^{15}\text{N}_\alpha$ values (Fig. 6), which originates from the wide range of $\delta^{15}\text{N}(\text{NO}_3^-)$ values (Fig. 7). Two options could 490 then be considered to justify the asymmetric nature of the intermediate whose exact chemical formula is unknown. Firstly, the precursor of the β -position N atom could be different from NH_2OH . Although most studies on hybrid N_2O production report a reaction between NH_2OH and NO_2^- , other nucleophilic precursors have been reported as precursors of hybrid N_2O . Hydrazine (N_2H_4), for example, forms the asymmetrical intermediate $\text{HO}-\text{N}=\text{N}-\text{NH}_2$ (Perron et al., 1976). The second 495 alternative is that hybrid N_2O is indeed produced from NH_2OH and NO_2^- , but the very low temperatures modify the intermediate species.

The same hybrid production mechanism proposed for in situ N_2O production in Antarctic ice may occur at Don Juan Pond (DJP), Antarctica. Like in ice cores, N_2O formation at DJP reported by Samarkin et al. (2010) occurs under very low 500 temperatures and involves NO_3^- and especially NO_2^- , with higher production rates for NO_2^- as precursor. The authors demonstrated that N_2O extracted from DJP soil is abiotically produced. Moreover, they measured very low and highly variable SP values at DJP, down to -45 ‰, which also fall outside the typical SP range. This variability in SP values and similar environmental conditions support the possibility of a shared, likely abiotic, mechanism of hybrid N_2O production in Antarctic ice and at DJP.



505 **Figure 8. Production mechanisms for single-precursor N₂O (a) and hybrid N₂O (b), (c).** Two mechanisms for hybrid N₂O production are proposed: panel (b) explains constant SP values, while panel (c), which explains the observed SP dependence on the $\delta^{15}\text{N}$ values of the precursor, likely represents the in situ production pathway. (b) Mechanism with a symmetric intermediate, here the *cis*-hyponitrous acid HONNOH. Depending on which N-O bond of the symmetric intermediate breaks, the NO₂-derived and NH₂OH-derived N atoms can each end up either in the central position (α) or in the terminal position (β) in N₂O. The percentage of molecules 1 and 2, and consequently the site preference, only reflects the preferential cleavage of the ¹⁴N-O bond over the ¹⁵N-O bond during the last step of N₂O formation. Therefore, hybrid N₂O exhibits a consistent site preference that is independent of the $\delta^{15}\text{N}$ values of the precursors (Heil et al., 2014). In this case the O atom is derived from one precursor or the other. (c) Mechanism with an asymmetric intermediate. In this case, the O atom and the central N atom (N_α) are always derived from NO₂⁻ and the terminal N atom (N_β) from NH₂OH. The two N atoms retain the $\delta^{15}\text{N}$ signatures of their individual precursors. The site preference is therefore variable, as it depends on the difference between the $\delta^{15}\text{N}$ values of the two precursors. This mechanism matches our observations but to our knowledge has not yet been reported in the literature. Note that the precursors and intermediates shown in this figure are only examples used to illustrate our point about SP values. It is one hypothesis among others for the mechanism of in situ N₂O production as the nitrogen source of the terminal nitrogen N_β in N₂O (in yellow) remains unknown. During in situ production, Fe²⁺ carried by dust may reduce NO₃⁻ to NO₂⁻ and act as the limiting factor once fully oxidized to Fe³⁺.

520 5.4 Source of oxygen in in situ N₂O

Considering an N-nitrosation pathway, the observed $\delta^{18}\text{O}(\text{N}_2\text{O}_{\text{in situ}})$ values might be explained by the combined processes of NO₃⁻ reduction and NO₂⁻ isotopic equilibration with H₂O (Casciotti et al., 2007). Since N-nitrosation typically involves NO₂⁻ rather than NO₃⁻, it is likely that NO₃⁻ is first reduced to NO₂⁻. Several studies have shown that NO₂⁻ is prone to exchange its O atoms with the O atoms of water molecules in aqueous solution (Bunton et al., 1959). The water from Antarctic ice is 525 strongly depleted in ¹⁸O, with $\delta^{18}\text{O}(\text{H}_2\text{O})$ values of approximately -62 ‰ at Vostok (Lorius et al., 1985), -56 ‰ at EDC (Landais, Amaelle and Stenni, Barbara, 2021), -42 ‰ at EDML (EPICA Community Members, 2010) and -42 ‰ as well at TG (Baggenstos et al., 2018). Thus, incorporation of O atoms from H₂O into N₂O through exchange with NO₂⁻ could explain the ¹⁸O depletion observed in in situ N₂O compared to NO₃⁻ in the EDML, EDC, and Vostok ice cores (Fig. 5). However, the $\delta^{18}\text{O}(\text{N}_2\text{O}_{\text{in situ}})$ values are not correlated to $\delta^{18}\text{O}(\text{H}_2\text{O})$ values and the difference between $\delta^{18}\text{O}(\text{N}_2\text{O}_{\text{in situ}})$ and $\delta^{18}\text{O}(\text{NO}_3^-)$ is



530 significantly larger at EDML than at EDC and Vostok. This may indicate an incomplete exchange of O atoms between NO_2^- and H_2O , with a larger fraction of exchanged O atoms at EDML than EDC and Vostok.

In contrast, $\delta^{18}\text{O}(\text{N}_2\text{O}_{\text{in situ}})$ values at TG are unexpectedly higher than $\delta^{18}\text{O}(\text{NO}_3^-)$, suggesting that oxygen exchange with water alone cannot explain the $\delta^{18}\text{O}(\text{N}_2\text{O}_{\text{in situ}})$ values. In this case, the observed enrichment in ^{18}O compared to NO_3^- might be due to the “branching effect” associated with NO_3^- reduction. This effect results from the incomplete incorporation of the 535 oxygen pool from NO_3^- to N_2O (Casotti et al., 2007). Indeed, only two out of three O atoms from NO_3^- are transferred into NO_2^- , then one out of two from NO_2^- to N_2O . Since ^{16}O atoms are preferentially lost, NO_2^- and N_2O become enriched in ^{18}O . For the abiotic reduction of NO_2^- to N_2O by Fe^{2+} , the branching effect results in positive isotope effect of about +30 ‰ at 25 °C (Buchwald et al., 2016) which is likely even larger at very low temperatures. Although the same branching effect probably occurs at EDC, Vostok, and EDML, the fraction of exchanged O atoms might be smaller at TG, making the 540 branching effect relatively more pronounced in the final $\delta^{18}\text{O}(\text{N}_2\text{O}_{\text{in situ}})$ values.

The reason why the fraction of exchanged O atoms would vary among ice cores is not fully understood. It likely depends on the relative rates of oxygen isotope equilibration and the N-nitrosation reaction, both of which are temperature- and pH-dependent. Casotti et al. (2007) showed that oxygen exchange is faster under acidic conditions, and Su et al. (2019) reported that low pH also accelerates abiotic nitrosation reactions. Therefore, the combination of different ice chemical 545 compositions and environmental conditions during the reaction could influence the fraction of O atoms exchanged between NO_2^- and H_2O .

While the relative contributions of oxygen exchange and branching effect to the $\delta^{18}\text{O}(\text{N}_2\text{O}_{\text{in situ}})$ values remain unclear, overall, these processes may mask the transfer of the original $\delta^{18}\text{O}(\text{NO}_3^-)$ signature into in situ N_2O .

5.5 Likelihood of an abiotic production of N_2O

550 In situ N_2O production in polar ice has often been attributed to microbial activity. Sowers (2001) reported two N_2O maxima in the Vostok ice core at around 150 ka that coincided with elevated bacterial counts. Similarly, Rohde et al. (2008) found that in the GISP2 Greenland ice core, most of the samples affected by in situ production were associated with large cell counts.

However, several observations challenge the hypothesis of a microbial in situ production. First, the correlation between 555 microbial counts and N_2O maxima may not be causal, as the dust content could be a confounding variable: mineral particles are the main carriers of microbial cells to the ice sheet (Miteva, 2008; Miteva et al., 2016), so both microbial concentrations and in situ N_2O are positively correlated with dust content in Antarctic ice cores. Second, because the low temperatures affect microbial metabolism and thus limit the reaction, one would expect the increase in ice temperature with depth to result in an increase in excess N_2O as well. However, such an increase is not observed (Schilt et al., 2010b). Third, microbial 560 activity generally requires the presence of liquid water. Although thin water channels called “liquid veins” can form during ice crystal growth due to concentration of acidic impurities at crystal interfaces (Barletta et al., 2012; Dani et al., 2012), the upper hundreds of meters where N_2O is produced are too cold for such features to exist at sites like Vostok (Dani et al.,



2012). Fourth, no functional genes involved in bacterial and archaeal nitrification and denitrification were detected by PCR amplification in the NEEM Greenland ice core during the last glacial period (Miteva et al., 2016). Finally, Antarctic ice is an
565 acidic environment (EPICA community members, 2004; Wolff et al., 1997), but the review by Spott et al. (2011) indicates that hybrid N₂O production by biotic nitrosation generally occurs under neutral pH conditions, within a range of 6 to 7.5. Only one study reported AOA production of hybrid N₂O at a moderately low pH of 5.5 (Jung et al., 2019). In contrast, Su et al. (2019) showed that abiotic production of hybrid N₂O is enhanced at pH ≤ 5. Given the above constraints, an abiotic mechanism is the most plausible explanation for in situ N₂O production.

570 An abiotic reaction triggered by low pH could explain the differences in N₂O production observed between Antarctic and Greenland ice. In Antarctic ice cores, N₂O production occurs consistently throughout dust-rich depths and the amount of in situ N₂O is roughly correlated with the amount of dust (Schilt et al., 2010b, a). In contrast, Greenland ice shows erratic N₂O production with a finite number of outliers of very high N₂O mixing ratio (Flückiger et al., 2004). In Greenland cores it occurs in specific depth intervals with moderate dust concentrations, while sections with very high dust concentrations rarely
575 show in situ production. This very dusty Greenland ice is alkaline due to the deposition of alkaline dust (calcium carbonates), which can neutralize acids in the ice (Biscaye et al., 1997; Mayewski et al., 1994; Wolff et al., 1997), a phenomenon not observed in Antarctic ice which is acidic (EPICA community members, 2004; Wolff et al., 1997). The generally higher pH of Greenland ice (Rasmussen et al., 2023) may inhibit in situ N₂O production, potentially explaining the absence of widespread production in these cores. Isolated outliers with elevated N₂O mixing ratios occur at depths where the
580 ice is more acidic, for instance near volcanic horizons, as they are often found close to sulfate peaks.

6 Conclusion

Using bulk and position-specific isotope analyses, we have improved the understanding of N₂O production in Antarctic ice while also raising new questions about its nature. Our results show that N₂O produced in ice is hybrid N₂O, with its central N atom (N_α) derived from NO₃⁻ and its terminal N atom (N_β) from a different precursor. This hybrid N₂O is likely produced
585 abiotically through an N-nitrosation reaction, in which NO₃⁻ is first reduced to NO₂⁻ that then reacts with a nucleophilic compound that supplies N_β in N₂O. Fe²⁺ contained in dust particles may be the agent that reduces NO₃⁻ to NO₂⁻. In addition to the precursor of the terminal N atom, this reducing agent could be a limiting factor in the reaction. Low pH may also be a necessary condition for this process. To better understand the pH control on N₂O production, future work should investigate the isolated in situ N₂O outliers in Greenland ice. The sources of the terminal N atom (N_β) and the O atom in in situ N₂O remain uncertain. One possibility is that N_β originates from NH₄⁺, potentially converted to NH₂OH; measuring the isotopic composition of NH₄⁺ in Antarctic ice cores could help test this hypothesis. For the O atom, it may be derived from two different oxygen pools – either from NO₃⁻ or from H₂O through oxygen exchange with NO₂⁻.

Our work revealed that the isotopic composition of in situ N₂O is highly variable even within a single ice core. As a result, N₂O records from ice cores cannot be accurately corrected for in situ production using a fixed isotopic signature in a mass

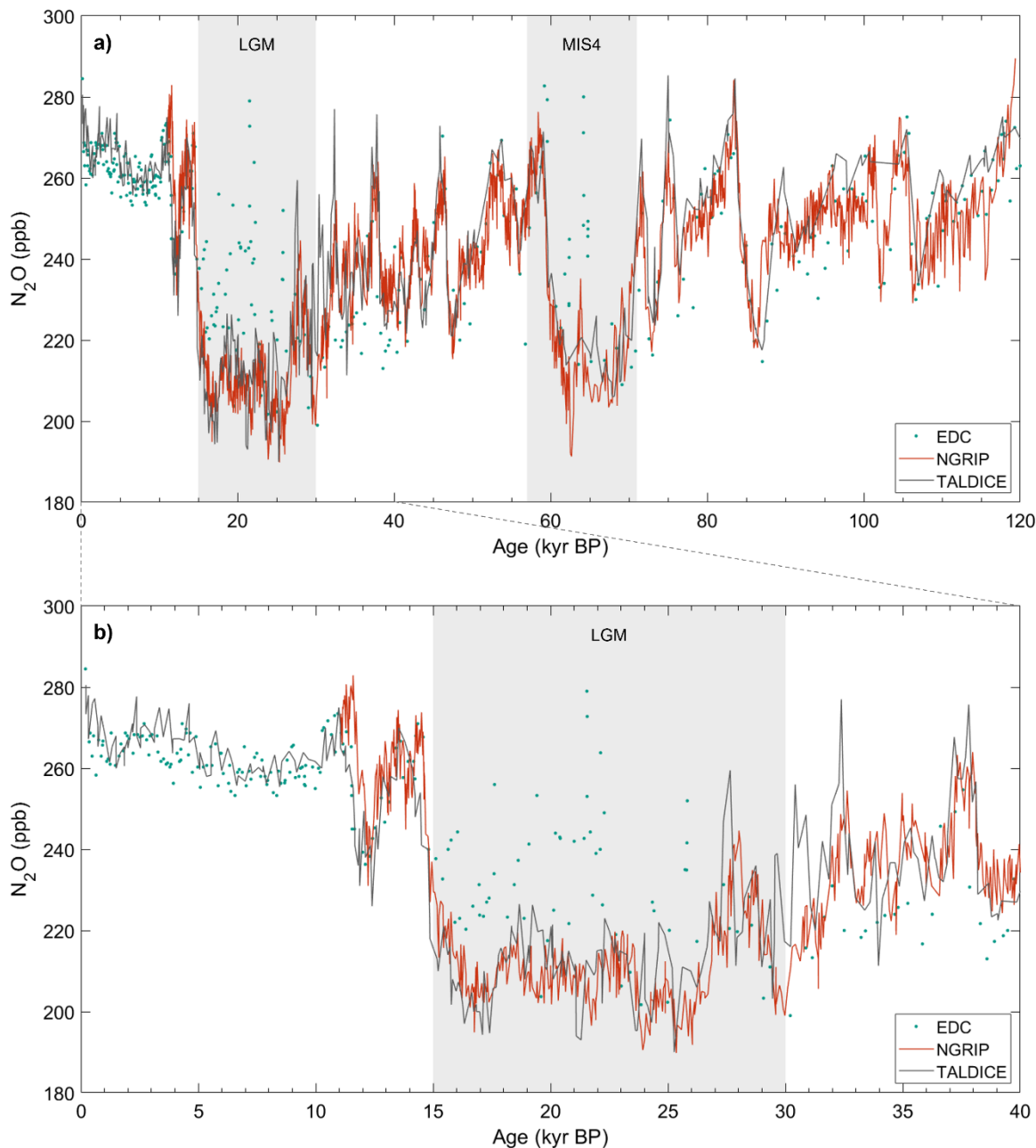


595 balance approach. A more robust correction method would be to measure NO_3^- isotopic composition alongside total N_2O in the same samples, as we did in this study. Since the in situ N_2O signature reflects the variability of NO_3^- isotopes, this method would help estimate the isotopic signature of in situ N_2O in affected samples. We could not apply this method to the existing N_2O records because the meltwater was not collected after N_2O analysis, thus the NO_3^- isotopic composition cannot be measured in these specific samples.

600 This study also highlights the importance of accounting for in situ N_2O production when using N_2O isotopes for source attribution. In some ice cores, the isotopic signature of in situ N_2O deviates drastically from the atmospheric signal. Even small amounts of in situ N_2O can significantly impact the measured isotopic composition and thus alter paleoclimatic interpretations. For example, for atmospheric N_2O at a mixing ratio of 200 ppb and in situ N_2O at 5 ppb, with $\delta^{15}\text{N}_{\text{bulk}}(\text{N}_2\text{O}_{\text{in situ}})$ as high as +70 ‰ as we observed in the Vostok ice core, this small in situ contribution would shift the $\delta^{15}\text{N}_{\text{bulk}}(\text{N}_2\text{O}_{\text{total}})$ by +1.5 ‰. Such a shift would result in a 16 % increase in estimated marine N_2O emissions and a change in marine-to-terrestrial emission ratio from 0.39 to 0.45, which is close to the entire change observed over the last 21 kyr (Fischer et al., 2019). Therefore, identifying and excluding all samples affected by in situ production is essential to avoid misinterpretation. Our results reveal a previously unidentified N_2O production pathway likely involving an asymmetric reaction intermediate. This process may not be limited to ice but could also occur in other environments such as soils or aquatic systems, 610 suggesting it may contribute to atmospheric N_2O more broadly. This has important implications for the interpretation of SP values. The $\text{SP}(\text{N}_2\text{O}_{\text{in situ}})$ values observed in this study show unusual variability and strong dependence on the isotopic composition of the precursors, compared to SP values reported in previous studies (Heil et al., 2014; Toyoda et al., 2017). These results may reflect the production of hybrid N_2O via an asymmetric intermediate, where N_α and N_β originate from 615 distinct precursors and retain the isotopic signature of their respective sources. In this case, the SP values depend on the difference between the isotopic signatures of the two sources. This mechanism complicates the use of SP to trace N_2O pathways, as they are not always characterized by a constant SP value. We therefore recommend further investigation of SP values in hybrid N_2O under different environmental conditions and reaction mechanisms.



Appendix A – Can the TALDICE data be used as an atmospheric reference?



620 **Figure A1.** N_2O concentrations measured in the TALDICE (Schilt et al., 2010a), NGRIP (Flückiger et al., 2004; Schilt et al., 2010a, 2013), and EDC (Schilt et al., 2010b) ice cores over the last 120 kyr (a) and over the last 40 kyr (b). In situ N_2O outliers have been removed from the NGRIP record. The EDC ice core is affected by in situ production of N_2O during the LGM and MIS4.



Appendix B – Uncertainties in the mass balance calculation

Table B1. Uncertainty ranges used in the Monte-Carlo calculation of the uncertainty of in situ N_2O isotopic signature. Here we report the uncertainties due to differences in gas age scales of TALDICE and other ice cores, as the atmospheric values in the mass balance calculation are defined as the spline values matching the age of the measured sample.

Variable	Uncertainty range
Gas age	0.7 kyr
N_2O concentration of the atmospheric spline	4 ppb
$\delta^{15}\text{N}$ values of the N_2O atmospheric spline	0.3 ‰
$\delta^{15}\text{N}_a$ value of atmospheric N_2O (Menking et al., 2025)	1.7 ‰
$\delta^{18}\text{O}$ values of the N_2O atmospheric spline	0.6 ‰
Measured N_2O concentration	4 ppb
Measured $\delta^{15}\text{N}(\text{N}_2\text{O})$ values	0.3 ‰
Measured $\delta^{15}\text{N}_a(\text{N}_2\text{O})$ values	0.6 ‰
Measured $\delta^{18}\text{O}(\text{N}_2\text{O})$ values	0.6 ‰

Appendix C – Sensitivity study: potential in situ contribution in TALDICE N_2O

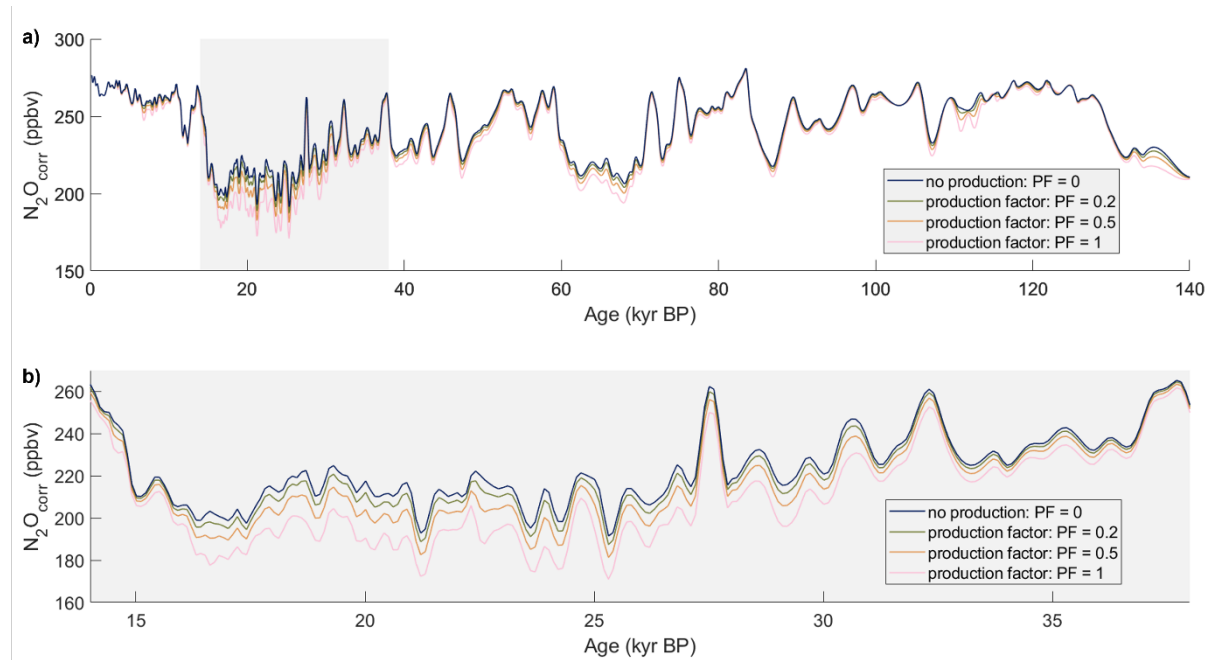
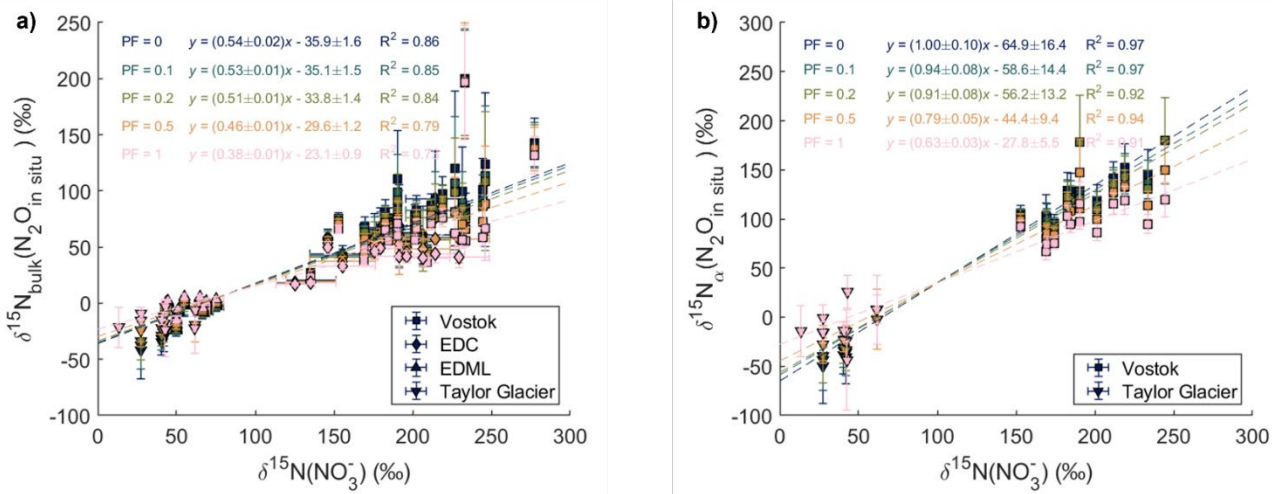




Figure C1. Spline interpolation of TALDICE N₂O concentrations, corrected for potential in situ production proportional to dust content. The different curves correspond to varying production factors, which link dust concentration to the amount of in situ N₂O produced. (a): 0 to 140 kyr BP, (b): 14 to 38 kyr BP.



635

Figure C2. Sensitivity study testing the impact of in situ N₂O production in TALDICE proportional to Ca²⁺ concentrations, with production factors (PF) ranging from 0 to 1. PF = 0 means no N₂O production. (a) Relation between $\delta^{15}\text{N}_{\text{bulk}}(\text{N}_2\text{O}_{\text{in situ}})$ and $\delta^{15}\text{N}(\text{NO}_3^-)$. (b) Relation between $\delta^{15}\text{N}_{\alpha}(\text{N}_2\text{O}_{\text{in situ}})$ and $\delta^{15}\text{N}(\text{NO}_3^-)$.

640 **Appendix D – Assessment of potential NO₃⁻ contamination, loss, or isotopic fractionation during N₂O extraction from ice core samples**

Table D1. NO₃⁻ concentration and isotopic composition of the same samples with and without N₂O extraction.

		NO ₃ ⁻ concentration (ng.g ⁻¹)		NO ₃ ⁻ isotopic composition			
				$\delta^{15}\text{N}$ (‰)		$\delta^{18}\text{O}$ (‰)	
		No N ₂ O extraction	After N ₂ O extraction	No N ₂ O extraction	After N ₂ O extraction	No N ₂ O extraction	After N ₂ O extraction
Ultrapure water with NO ₃ ⁻ isotopic standard USGS32 (Bohlke et al., 1993)		80	75.2	+180 (reference value)	+175.7 ± 0.5	+25.4 ± 0.2 (reference value)	+34.7 ± 1.7
Duplicate ice core samples	B37 108	55.7	53.0	51.9 ± 0.4	54.8 ± 0.4	48.4 ± 2.3	59.2 ± 2.3
	EDC 1841	35.6	35.1	175.8 ± 0.5	176.0 ± 0.4	38.2 ± 1.7	40.5 ± 2.3



	EDML 1768	93.0	90.3	46.9 ± 0.4	50.9 ± 0.4	76.1 ± 2.3	84.1 ± 2.3
	EDML 976	64.8	64.6	63.3 ± 0.5	65.0 ± 0.5	78.5 ± 1.7	93.9 ± 1.7

Data Availability.

645 The data presented in this study will be available on PANGAEA.

Author Contribution.

The concept of the study was developed by JSc, HF, and LS. The bulk isotope analyses of N₂O were carried out by LS and BS. LS performed the position-specific isotope analyses of N₂O under the guidance of JM and EB and the NO₃⁻ isotope analyses under the guidance of JSa. JSa, VL, and EB provided ice core samples. LS and JSc analyzed the data. TR, JM, and 650 EB provided input on SP measurements. HF managed and supervised the project. LS wrote the manuscript with contributions from all authors.

Competing interests.

The contact author has declared that none of the authors has any competing interests.

Financial support.

655 This research has been supported by the Horizon 2020 research and innovation programme (grant no. 955750) and by the Swiss National Science Foundation (grant no. 200020_200328).

References

Aarons, S. M., Aciego, S. M., Arendt, C. A., Blakowski, M. A., Steigmeyer, A., Gabrielli, P., Sierra-Hernández, M. R., Beaudon, E., Delmonte, B., Baccolini, G., May, N. W., and Pratt, K. A.: Dust composition changes from Taylor Glacier (East 660 Antarctica) during the last glacial-interglacial transition: A multi-proxy approach, Quaternary Science Reviews, 162, 60–71, <https://doi.org/10.1016/j.quascirev.2017.03.011>, 2017.



Anklin, M., Barnola, J.-M., Schwander, J., Stauffer, B., and Raynaud, D.: Processes affecting the CO₂ concentrations measured in Greenland ice, *Tellus B*, 47, 461–470, <https://doi.org/10.1034/j.1600-0889.47.issue4.6.x>, 1995.

Baccolo, G., Delmonte, B., Niles, P. B., Cibin, G., Di Stefano, E., Hampai, D., Keller, L., Maggi, V., Marcelli, A.,
665 Michalski, J., Snead, C., and Frezzotti, M.: Jarosite formation in deep Antarctic ice provides a window into acidic, water-limited weathering on Mars, *Nat Commun*, 12, 436, <https://doi.org/10.1038/s41467-020-20705-z>, 2021.

Baggenstos, D., Severinghaus, J. P., Mulvaney, R., McConnell, J. R., Sigl, M., Maselli, O., Petit, J., Grente, B., and Steig, E. J.: A Horizontal Ice Core From Taylor Glacier, Its Implications for Antarctic Climate History, and an Improved Taylor Dome Ice Core Time Scale, *Paleoceanog and Paleoclimatol*, 33, 778–794, <https://doi.org/10.1029/2017PA003297>, 2018.

670 Baggs, E. M.: Soil microbial sources of nitrous oxide: recent advances in knowledge, emerging challenges and future direction, *Current Opinion in Environmental Sustainability*, 3, 321–327, <https://doi.org/10.1016/j.cosust.2011.08.011>, 2011.

Bange, H. W.: Gaseous Nitrogen Compounds (NO, N₂O, N₂, NH₃) in the Ocean, in: *Nitrogen in the Marine Environment*, Elsevier, 51–94, <https://doi.org/10.1016/B978-0-12-372522-6.00002-5>, 2008.

Barletta, R. E., Priscu, J. C., Mader, H. M., Jones, W. L., and Roe, C. H.: Chemical analysis of ice vein microenvironments: II. Analysis of glacial samples from Greenland and Antarctica, *J. Glaciol.*, 58, 1109–1118, <https://doi.org/10.3189/2012JoG12J112>, 2012.

Battle, M., Bender, M., Sowers, T., Tans, P. P., Butler, J. H., Elkins, J. W., Ellis, J. T., Conway, T., Zhang, N., Lang, P., and Clarket, A. D.: Atmospheric gas concentrations over the past century measured in air from firn at the South Pole, *Nature*, 383, 231–235, <https://doi.org/10.1038/383231a0>, 1996.

680 Bernard, S., Röckmann, T., Kaiser, J., Barnola, J.-M., Fischer, H., Blunier, T., and Chappellaz, J.: Constraints on N₂O budget changes since pre-industrial time from new firn air and ice core isotope measurements, *Atmos. Chem. Phys.*, 6, 493–503, <https://doi.org/10.5194/acp-6-493-2006>, 2006.

Bigler, M.: Hochauflösende Spurenstoffmessungen an polaren Eisbohrkernen: Glazio-chemische und klimatische Prozessstudien, <https://doi.org/10.57694/7211>, 2024.

685 Biscaye, P. E., Grousset, F. E., Revel, M., Van Der Gaast, S., Zielinski, G. A., Vaars, A., and Kukla, G.: Asian provenance of glacial dust (stage 2) in the Greenland Ice Sheet Project 2 Ice Core, Summit, Greenland, *J. Geophys. Res.*, 102, 26765–26781, <https://doi.org/10.1029/97JC01249>, 1997.

Blunier, T., Floch, G. L., Jacobi, H., and Quansah, E.: Isotopic view on nitrate loss in Antarctic surface snow, *Geophysical Research Letters*, 32, 2005GL023011, <https://doi.org/10.1029/2005GL023011>, 2005.

690 Bohlke, J. K., Gwinn, C. J., and Coplen, T. B.: New reference materials for nitrogen-isotope-ratio measurements, *Geostandards and Geoanalytical Research*, 17, 159–164, <https://doi.org/10.1111/j.1751-908X.1993.tb00131.x>, 1993.

Bouchet, M., Landais, A., Grisart, A., Parrenin, F., Prié, F., Jacob, R., Fourré, E., Capron, E., Raynaud, D., Lipenkov, V. Y., Loutre, M.-F., Extier, T., Svensson, A. M., Martinerie, P., Leuenberger, M. C., Jiang, W., Ritterbusch, F., Lu, Z.-T., and Yang, G.-M.: The Antarctic ice core chronology (AICC2023), <https://doi.org/10.1594/PANGAEA.961017>, 2023.



695 Buchwald, C., Grabb, K., Hansel, C. M., and Wankel, S. D.: Constraining the role of iron in environmental nitrogen transformations: Dual stable isotope systematics of abiotic NO₂– reduction by Fe(II) and its production of N₂O, *Geochimica et Cosmochimica Acta*, 186, 1–12, <https://doi.org/10.1016/j.gca.2016.04.041>, 2016.

700 Buiron, D., Chappellaz, J., Stenni, B., Frezzotti, M., Baumgartner, M., Capron, E., Landais, A., Lemieux-Dudon, B., Masson-Delmotte, V., Montagnat, M., Parrenin, F., and Schilt, A.: TALDICE-1 age scale of the Talos Dome deep ice core, *East Antarctica, Clim. Past*, 7, 1–16, <https://doi.org/10.5194/cp-7-1-2011>, 2011.

Bunton, C. A., Llewellyn, D. R., and Stedman, G.: Oxygen exchange between nitrous acid and water, *J. Chem. Soc.*, 568, <https://doi.org/10.1039/jr9590000568>, 1959.

Casciotti, K. L., Böhlke, J. K., McIlvin, M. R., Mroczkowski, S. J., and Hannon, J. E.: Oxygen Isotopes in Nitrite: Analysis, Calibration, and Equilibration, *Anal. Chem.*, 79, 2427–2436, <https://doi.org/10.1021/ac061598h>, 2007.

705 Chen, Z.-L., Song, W., Hu, C.-C., Liu, X.-J., Chen, G.-Y., Walters, W. W., Michalski, G., Liu, C.-Q., Fowler, D., and Liu, X.-Y.: Significant contributions of combustion-related sources to ammonia emissions, *Nat Commun*, 13, 7710, <https://doi.org/10.1038/s41467-022-35381-4>, 2022.

710 Crotti, I., Landais, A., Stenni, B., Bazin, L., Parrenin, F., Frezzotti, M., Ritterbusch, F., Lu, Z.-T., Jiang, W., Yang, G.-M., Fourré, E., Orsi, A., Jacob, R., Minster, B., Prié, F., Dreossi, G., and Barbante, C.: An extension of the TALDICE ice core age scale reaching back to MIS 10.1, *Quaternary Science Reviews*, 266, 107078, <https://doi.org/10.1016/j.quascirev.2021.107078>, 2021.

Dani, K. G. S., Mader, H. M., Wolff, E. W., and Wadham, J. L.: Modelling the liquid-water vein system within polar ice sheets as a potential microbial habitat, *Earth and Planetary Science Letters*, 333–334, 238–249, <https://doi.org/10.1016/j.epsl.2012.04.009>, 2012.

715 Delmas, R. J.: A natural artefact in Greenland ice-core CO₂ measurements, *Tellus B*, 45, 391–396, <https://doi.org/10.1034/j.1600-0889.1993.t01-3-00006.x>, 1993.

Delmonte, B., Basile-Doelsch, I., Petit, J.-R., Maggi, V., Revel-Rolland, M., Michard, A., Jagoutz, E., and Grousset, F.: Comparing the Epica and Vostok dust records during the last 220,000 years: stratigraphical correlation and provenance in glacial periods, *Earth-Science Reviews*, 66, 63–87, <https://doi.org/10.1016/j.earscirev.2003.10.004>, 2004.

720 Delmonte, B., Baroni, C., Andersson, P. S., Schoberg, H., Hansson, M., Aciego, S., Petit, J., Albani, S., Mazzola, C., Maggi, V., and Frezzotti, M.: Aeolian dust in the Talos Dome ice core (East Antarctica, Pacific/Ross Sea sector): Victoria Land *versus* remote sources over the last two climate cycles, *J Quaternary Science*, 25, 1327–1337, <https://doi.org/10.1002/jqs.1418>, 2010.

EPICA community members: Eight glacial cycles from an Antarctic ice core, *Nature*, 429, 623–628, <https://doi.org/10.1038/nature02599>, 2004.

725 EPICA Community Members: Stable oxygen isotopes of ice core EDML, <https://doi.org/10.1594/PANGAEA.754444>, 2010.

Erbland, J.: Contraintes isotopiques sur l'interprétation de l'enregistrement en nitrate dans la carotte de glace de Vostok, Université de Grenoble, 2011.



730 Erbland, J., Vicars, W. C., Savarino, J., Morin, S., Frey, M. M., Frosini, D., Vince, E., and Martins, J. M. F.: Air–snow transfer of nitrate on the East Antarctic Plateau – Part 1: Isotopic evidence for a photolytically driven dynamic equilibrium in summer, *Atmos. Chem. Phys.*, 13, 6403–6419, <https://doi.org/10.5194/acp-13-6403-2013>, 2013.

735 Fischer, H., Fundel, F., Ruth, U., Twarloh, B., Wegner, A., Udisti, R., Becagli, S., Castellano, E., Morganti, A., Severi, M., Wolff, E., Littot, G., Röthlisberger, R., Mulvaney, R., Hutterli, M. A., Kaufmann, P., Federer, U., Lambert, F., Bigler, M., Hansson, M., Jonsell, U., De Angelis, M., Boutron, C., Siggaard-Andersen, M.-L., Steffensen, J. P., Barbante, C., Gaspari, V., Gabrielli, P., and Wagenbach, D.: Reconstruction of millennial changes in dust emission, transport and regional sea ice coverage using the deep EPICA ice cores from the Atlantic and Indian Ocean sector of Antarctica, *Earth and Planetary Science Letters*, 260, 340–354, <https://doi.org/10.1016/j.epsl.2007.06.014>, 2007.

740 Fischer, H., Schmitt, J., Bock, M., Seth, B., Joos, F., Spahni, R., Lienert, S., Battaglia, G., Stocker, B. D., Schilt, A., and Brook, E. J.: N₂O changes from the Last Glacial Maximum to the preindustrial – Part 1: Quantitative reconstruction of terrestrial and marine emissions using N₂O stable isotopes in ice cores, *Biogeosciences*, 16, 3997–4021, <https://doi.org/10.5194/bg-16-3997-2019>, 2019.

745 Flückiger, J., Monnin, E., Stauffer, B., Schwander, J., Stocker, T. F., Chappellaz, J., Raynaud, D., and Barnola, J.-M.: High-resolution Holocene N₂O ice core record and its relationship with CH₄ and CO₂: High-resolution Holocene N₂O ice core record, *Global Biogeochem. Cycles*, 16, 10-1-10-8, <https://doi.org/10.1029/2001GB001417>, 2002.

750 Flückiger, J., Blunier, T., Stauffer, B., Chappellaz, J., Spahni, R., Kawamura, K., Schwander, J., Stocker, T. F., and Dahl-Jensen, D.: N₂O and CH₄ variations during the last glacial epoch: Insight into global processes., *Global Biogeochem. Cycles*, 18, n/a-n/a, <https://doi.org/10.1029/2003GB002122>, 2004.

755 Frame, C. H. and Casciotti, K. L.: Biogeochemical controls and isotopic signatures of nitrous oxide production by a marine ammonia-oxidizing bacterium, *Biogeosciences*, 7, 2695–2709, <https://doi.org/10.5194/bg-7-2695-2010>, 2010.

760 Frey, M. M., Savarino, J., Morin, S., Erbland, J., and Martins, J. M. F.: Photolysis imprint in the nitrate stable isotope signal in snow and atmosphere of East Antarctica and implications for reactive nitrogen cycling, *Atmos. Chem. Phys.*, 9, 8681–8696, <https://doi.org/10.5194/acp-9-8681-2009>, 2009.

Fuhrer, K., Wolff, E., and Johnsen, S. J.: Timescales for dust variability in the Greenland Ice Core Project (GRIP) ice core in the last 100,000 years, *J. Geophys. Res.*, 104, 31043–31052, <https://doi.org/10.1029/1999JD900929>, 1999.

765 Gruber, N. and Galloway, J. N.: An Earth-system perspective of the global nitrogen cycle, *Nature*, 451, 293–296, <https://doi.org/10.1038/nature06592>, 2008.

Heil, J., Wolf, B., Brüggemann, N., Emmenegger, L., Tuzson, B., Vereecken, H., and Mohn, J.: Site-specific ¹⁵N isotopic signatures of abiotically produced N₂O, *Geochimica et Cosmochimica Acta*, 139, 72–82, <https://doi.org/10.1016/j.gca.2014.04.037>, 2014.

770 Heil, J., Liu, S., Vereecken, H., and Brüggemann, N.: Abiotic nitrous oxide production from hydroxylamine in soils and their dependence on soil properties, *Soil Biology and Biochemistry*, 84, 107–115, <https://doi.org/10.1016/j.soilbio.2015.02.022>, 2015.



Herron, M. M. and Langway, C. C.: Firn Densification: An Empirical Model, *J. Glaciol.*, 25, 373–385, <https://doi.org/10.3189/S0022143000015239>, 1980.

765 IPCC: Climate Change 2021: The Physical Science Basis. Contribution of Working Group I to the Sixth Assessment Report of the Intergovernmental Panel on Climate Change, In Press, <https://doi.org/10.1017/9781009157896>, 2021.

Jones, L. C., Peters, B., Lezama Pacheco, J. S., Casciotti, K. L., and Fendorf, S.: Stable Isotopes and Iron Oxide Mineral Products as Markers of Chemodenitrification., *Environ. Sci. Technol.*, 49, 3444–3452, <https://doi.org/10.1021/es504862x>, 2015.

770 Jung, M.-Y., Gwak, J.-H., Rohe, L., Giesemann, A., Kim, J.-G., Well, R., Madsen, E. L., Herbold, C. W., Wagner, M., and Rhee, S.-K.: Indications for enzymatic denitrification to N₂O at low pH in an ammonia-oxidizing archaeon, *The ISME Journal*, 13, 2633–2638, <https://doi.org/10.1038/s41396-019-0460-6>, 2019.

Kaiser, J., Hastings, M. G., Houlton, B. Z., Röckmann, T., and Sigman, D. M.: Triple Oxygen Isotope Analysis of Nitrate Using the Denitrifier Method and Thermal Decomposition of N₂O, *Anal. Chem.*, 79, 599–607, <https://doi.org/10.1021/ac061022s>, 2007.

Kaufmann, P., Fundel, F., Fischer, H., Bigler, M., Ruth, U., Udisti, R., Hansson, M., de Angelis, M., Barbante, C., Wolff, E. W., Hutterli, M., and Wagenbach, D.: Ammonium and non-sea salt sulfate in the EPICA ice cores as indicator of biological activity in the Southern Ocean, *Quaternary Science Reviews*, 29, 313–323, <https://doi.org/10.1016/j.quascirev.2009.11.009>, 2010.

780 Kindler, P., Guillevic, M., Baumgartner, M., Schwander, J., Landais, A., and Leuenberger, M.: Temperature reconstruction from 10 to 120 kyr b2k from the NGRIP ice core, *Clim. Past*, 10, 887–902, <https://doi.org/10.5194/cp-10-887-2014>, 2014.

Lambert, F., Bigler, M., Steffensen, J. P., Hutterli, M., and Fischer, H.: Centennial mineral dust variability in high-resolution ice core data from Dome C, Antarctica, *Clim. Past*, 8, 609–623, <https://doi.org/10.5194/cp-8-609-2012>, 2012.

785 Lamothe, A., Savarino, J., Ginot, P., Soussaintjean, L., Gautier, E., Akers, P. D., Caillon, N., and Erbland, J.: An extraction method for nitrogen isotope measurement of ammonium in a low-concentration environment, *Atmos. Meas. Tech.*, 16, 4015–4030, <https://doi.org/10.5194/amt-16-4015-2023>, 2023.

Lan, X., Thoning, K., Dlugokencky, E., and NOAA Global Monitoring Laboratory: Trends in globally-averaged CH₄, N₂O, and SF₆ determined from NOAA Global Monitoring Laboratory measurements (Version 2025-04), <https://doi.org/10.15138/P8XG-AA10>, 2025.

790 Landais, Amaelle and Stenni, Barbara: Water stable isotopes (dD, d¹⁸O) from EPICA Dome C ice core (Antarctica) (0–800 ka), <https://doi.org/10.1594/PANGAEA.934094>, 2021.

Lee, J. E., Edwards, J. S., Schmitt, J., Fischer, H., Bock, M., and Brook, E. J.: Excess methane in Greenland ice cores associated with high dust concentrations, *Geochimica et Cosmochimica Acta*, 270, 409–430, <https://doi.org/10.1016/j.gca.2019.11.020>, 2020.

795 Lorius, C., Jouzel, J., Ritz, C., Merlivat, L., Barkov, N. I., Korotkevitch, Y. S., and Kotlyakov, V.: Delta 18O record versus age for 150 ka in ice core Vostok, <https://doi.org/10.1594/PANGAEA.860950>, 1985.



Louergue, L., Schilt, A., Spahni, R., Masson-Delmotte, V., Blunier, T., Lemieux, B., Barnola, J.-M., Raynaud, D., Stocker, T. F., and Chappellaz, J.: Orbital and millennial-scale features of atmospheric CH₄ over the past 800,000 years, *Nature*, 453, 383–386, <https://doi.org/10.1038/nature06950>, 2008.

800 Lüthi, D., Le Floch, M., Bereiter, B., Blunier, T., Barnola, J.-M., Siegenthaler, U., Raynaud, D., Jouzel, J., Fischer, H., Kawamura, K., and Stocker, T. F.: High-resolution carbon dioxide concentration record 650,000–800,000 years before present, *Nature*, 453, 379–382, <https://doi.org/10.1038/nature06949>, 2008.

Marino, F., Castellano, E., Nava, S., Chiari, M., Ruth, U., Wegner, A., Lucarelli, F., Udisti, R., Delmonte, B., and Maggi, V.: Coherent composition of glacial dust on opposite sides of the East Antarctic Plateau inferred from the deep EPICA ice cores, 805 *Geophysical Research Letters*, 36, 2009GL040732, <https://doi.org/10.1029/2009GL040732>, 2009.

Markle, B. R. and Steig, E. J.: Improving temperature reconstructions from ice-core water-isotope records, *Clim. Past*, 18, 1321–1368, <https://doi.org/10.5194/cp-18-1321-2022>, 2022.

Mayewski, P. A., Meeker, L. D., Whitlow, S., Twickler, M. S., Morrison, M. C., Bloomfield, P., Bond, G. C., Alley, R. B., Gow, A. J., Meese, D. A., Grootes, P. M., Ram, M., Taylor, K. C., and Wumkes, W.: Changes in Atmospheric Circulation 810 and Ocean Ice Cover over the North Atlantic During the Last 41,000 Years, *Science*, 263, 1747–1751, <https://doi.org/10.1126/science.263.5154.1747>, 1994.

Menking, J. A., Brook, E. J., Schilt, A., Shackleton, S., Dyonisius, M., Severinghaus, J. P., and Petrenko, V. V.: Millennial-Scale Changes in Terrestrial and Marine Nitrous Oxide Emissions at the Onset and Termination of Marine Isotope Stage 4, *Geophysical Research Letters*, 47, <https://doi.org/10.1029/2020GL089110>, 2020.

815 Menking, J. A., Lee, J. E., Brook, E. J., Schmitt, J., Soussaintjean, L., Fischer, H., Kaiser, J., and Rice, A.: Glacial-Interglacial and Millennial-Scale Changes in Nitrous Oxide Emissions Pathways and Source Regions, *Global Biogeochemical Cycles*, 39, e2024GB008287, <https://doi.org/10.1029/2024GB008287>, 2025.

Miteva, V.: Bacteria in Snow and Glacier Ice, in: *Psychrophiles: from Biodiversity to Biotechnology*, edited by: Margesin, R., Schinner, F., Marx, J.-C., and Gerday, C., Springer Berlin Heidelberg, Berlin, Heidelberg, 31–50, 820 https://doi.org/10.1007/978-3-540-74335-4_3, 2008.

Miteva, V., Sowers, T., and Brenchley, J.: Production of N₂O by Ammonia Oxidizing Bacteria at Subfreezing Temperatures as a Model for Assessing the N₂O Anomalies in the Vostok Ice Core, *Geomicrobiology Journal*, 24, 451–459, <https://doi.org/10.1080/01490450701437693>, 2007.

825 Miteva, V., Sowers, T., Schüpbach, S., Fischer, H., and Brenchley, J.: Geochemical and Microbiological Studies of Nitrous Oxide Variations within the New NEEM Greenland Ice Core during the Last Glacial Period, *Geomicrobiology Journal*, 33, 647–660, <https://doi.org/10.1080/01490451.2015.1074321>, 2016.

Morin, S., Savarino, J., Frey, M. M., Domine, F., Jacobi, H.-W., Kaleschke, L., and Martins, J. M. F.: Comprehensive isotopic composition of atmospheric nitrate in the Atlantic Ocean boundary layer from 65°S to 79°N, *J. Geophys. Res.*, 114, D05303, <https://doi.org/10.1029/2008JD010696>, 2009.



830 Mühl, M., Schmitt, J., Seth, B., Lee, J. E., Edwards, J. S., Brook, E. J., Blunier, T., and Fischer, H.: Methane, ethane, and propane production in Greenland ice core samples and a first isotopic characterization of excess methane, *Clim. Past*, 19, 999–1025, <https://doi.org/10.5194/cp-19-999-2023>, 2023.

Perron, J. R., Stedman, G., and Uysal, N.: Kinetic and product study of the reaction between nitrous acid and hydrazine, *J. Chem. Soc., Dalton Trans.*, 2058, <https://doi.org/10.1039/dt9760002058>, 1976.

835 Prather, M. J., Hsu, J., DeLuca, N. M., Jackman, C. H., Oman, L. D., Douglass, A. R., Fleming, E. L., Strahan, S. E., Steenrod, S. D., Søvde, O. A., Isaksen, I. S. A., Froidevaux, L., and Funke, B.: Measuring and modeling the lifetime of nitrous oxide including its variability, *J. Geophys. Res. Atmos.*, 120, 5693–5705, <https://doi.org/10.1002/2015JD023267>, 2015.

840 Priscu, J. C., Christner, B. C., Dore, J. E., Popp, B. N., Casciotti, K. L., and Lyons, W. B.: Supersaturated N₂O in a perennially ice-covered Antarctic lake: Molecular and stable isotopic evidence for a biogeochemical relict, *Limnology & Oceanography*, 53, 2439–2450, <https://doi.org/10.4319/lo.2008.53.6.2439>, 2008.

845 Prokopiou, M., Martinerie, P., Sapart, C. J., Witrant, E., Monteil, G., Ishijima, K., Bernard, S., Kaiser, J., Levin, I., Blunier, T., Etheridge, D., Dlugokencky, E., Van De Wal, R. S. W., and Röckmann, T.: Constraining N₂O emissions since 1940 using firm air isotope measurements in both hemispheres, *Atmos. Chem. Phys.*, 17, 4539–4564, <https://doi.org/10.5194/acp-17-4539-2017>, 2017.

Prokopiou, M., Sapart, C. J., Rosen, J., Sperlich, P., Blunier, T., Brook, E., Van De Wal, R. S. W., and Röckmann, T.: Changes in the Isotopic Signature of Atmospheric Nitrous Oxide and Its Global Average Source During the Last Three Millennia, *JGR Atmospheres*, 123, <https://doi.org/10.1029/2018JD029008>, 2018.

850 Rasmussen, S. O., Dahl-Jensen, D., Fischer, H., Fuhrer, K., Hansen, S. B., Hansson, M., Hvidberg, C. S., Jonsell, U., Kipfstuhl, S., Ruth, U., Schwander, J., Siggaard-Andersen, M.-L., Sinnl, G., Steffensen, J. P., Svensson, A. M., and Vinther, B. M.: Ice-core data used for the construction of the Greenland Ice-Core Chronology 2005 and 2021 (GICC05 and GICC21), *Earth Syst. Sci. Data*, 15, 3351–3364, <https://doi.org/10.5194/essd-15-3351-2023>, 2023.

Ravishankara, A. R., Daniel, J. S., and Portmann, R. W.: Nitrous Oxide (N₂O): The Dominant Ozone-Depleting Substance Emitted in the 21st Century, *Science*, 326, 123–125, <https://doi.org/10.1126/science.1176985>, 2009.

855 Ritz, C., Lliboutry, L., and Rado, C.: Analysis of a 870 m deep temperature profile at Dome C, *Annals of Glaciology*, 3, 284–289, 1982.

Rohde, R. A., Price, P. B., Bay, R. C., and Bramall, N. E.: In situ microbial metabolism as a cause of gas anomalies in ice, *Proceedings of the National Academy of Sciences*, 105, 8667–8672, <https://doi.org/10.1073/pnas.0803763105>, 2008.

Röthlisberger, R., Hutterli, M. A., Sommer, S., Wolff, E. W., and Mulvaney, R.: Factors controlling nitrate in ice cores: Evidence from the Dome C deep ice core, *J. Geophys. Res.*, 105, 20565–20572, <https://doi.org/10.1029/2000JD900264>, 2000.



Rubasinghege, G., Spak, S. N., Stanier, C. O., Carmichael, G. R., and Grassian, V. H.: Abiotic Mechanism for the Formation of Atmospheric Nitrous Oxide from Ammonium Nitrate, *Environ. Sci. Technol.*, 45, 2691–2697, <https://doi.org/10.1021/es103295v>, 2011.

865 Rubino, M., Etheridge, D. M., Thornton, D. P., Howden, R., Allison, C. E., Francey, R. J., Langenfelds, R. L., Steele, L. P., Trudinger, C. M., Spencer, D. A., Curran, M. A. J., Van Ommen, T. D., and Smith, A. M.: Revised records of atmospheric trace gases CO₂, CH₄, N₂O, and $\delta^{13}\text{C}$ -CO₂ over the last 2000 years from Law Dome, Antarctica, *Earth Syst. Sci. Data*, 11, 473–492, <https://doi.org/10.5194/essd-11-473-2019>, 2019.

870 Ruth, U., Wagenbach, D., Bigler, M., Steffensen, J. P., Röthlisberger, R., and Miller, H.: High-resolution microparticle profiles at NorthGRIP, Greenland: case studies of the calcium–dust relationship, *Ann. Glaciol.*, 35, 237–242, <https://doi.org/10.3189/172756402781817347>, 2002.

Ruth, U., Wagenbach, D., Steffensen, J. P., and Bigler, M.: Continuous record of microparticle concentration and size distribution in the central Greenland NGRIP ice core during the last glacial period, *J. Geophys. Res.*, 108, 2002JD002376, <https://doi.org/10.1029/2002JD002376>, 2003.

875 Salamatin, A. N., Lipenkov, V. Y., and Blinov, K. V.: Vostok (Antarctica) climate record time-scale deduced from the analysis of a borehole-temperature profile, *Annals of Glaciology*, 20, 207–214, 1994.

Samarkin, V. A., Madigan, M. T., Bowles, M. W., Casciotti, K. L., Priscu, J. C., McKay, C. P., and Joye, S. B.: Abiotic nitrous oxide emission from the hypersaline Don Juan Pond in Antarctica, *Nature Geosci.*, 3, 341–344, <https://doi.org/10.1038/ngeo847>, 2010.

880 Schilt, A., Baumgartner, M., Schwander, J., Buiron, D., Capron, E., Chappellaz, J., Louergue, L., Schüpbach, S., Spahni, R., Fischer, H., and Stocker, T. F.: Atmospheric nitrous oxide during the last 140,000 years, *Earth and Planetary Science Letters*, 300, 33–43, <https://doi.org/10.1016/j.epsl.2010.09.027>, 2010a.

Schilt, A., Baumgartner, M., Blunier, T., Schwander, J., Spahni, R., Fischer, H., and Stocker, T. F.: Glacial–interglacial and millennial-scale variations in the atmospheric nitrous oxide concentration during the last 800,000 years, *Quaternary Science Reviews*, 29, 182–192, <https://doi.org/10.1016/j.quascirev.2009.03.011>, 2010b.

885 Schilt, A., Baumgartner, M., Eicher, O., Chappellaz, J., Schwander, J., Fischer, H., and Stocker, T. F.: The response of atmospheric nitrous oxide to climate variations during the last glacial period, *Geophysical Research Letters*, 40, 1888–1893, <https://doi.org/10.1002/grl.50380>, 2013.

Schilt, A., Brook, E. J., Bauska, T. K., Baggenstos, D., Fischer, H., Joos, F., Petrenko, V. V., Schaefer, H., Schmitt, J., 890 Severinghaus, J. P., Spahni, R., and Stocker, T. F.: Isotopic constraints on marine and terrestrial N₂O emissions during the last deglaciation, *Nature*, 516, 234–237, <https://doi.org/10.1038/nature13971>, 2014.

Schmitt, J., Seth, B., Bock, M., and Fischer, H.: Online technique for isotope and mixing ratios of CH₄, N₂O, Xe and mixing ratios of organic trace gases on a single ice core sample, *Atmos. Meas. Tech.*, 7, 2645–2665, <https://doi.org/10.5194/amt-7-2645-2014>, 2014.



895 Schüpbach, S., Federer, U., Kaufmann, P. R., Albani, S., Barbante, C., Stocker, T. F., and Fischer, H.: Calcium and sodium concentrations of the Talos Dome ice core, Antarctica, <https://doi.org/10.1594/PANGAEA.833044>, 2014.

Sowers, T.: N₂O record spanning the penultimate deglaciation from the Vostok ice core, *J. Geophys. Res.*, 106, 31903–31914, <https://doi.org/10.1029/2000JD900707>, 2001.

900 Spahni, R., Chappellaz, J., Stocker, T. F., Loulergue, L., Hausmann, G., Kawamura, K., Flückiger, J., Schwander, J., Raynaud, D., Masson-Delmotte, V., and Jouzel, J.: Atmospheric Methane and Nitrous Oxide of the Late Pleistocene from Antarctic Ice Cores, *Science*, 310, 1317–1321, <https://doi.org/10.1126/science.1120132>, 2005.

Spolaor, A., Valletlonga, P., Gabrieli, J., Cozzi, G., Boutron, C., and Barbante, C.: Determination of Fe²⁺ and Fe³⁺ species by FIA-CRC-ICP-MS in Antarctic ice samples, *J. Anal. At. Spectrom.*, 27, 310–317, <https://doi.org/10.1039/C1JA10276A>, 2012.

905 Spolaor, A., Valletlonga, P., Cozzi, G., Gabrieli, J., Varin, C., Kehrwald, N., Zennaro, P., Boutron, C., and Barbante, C.: Iron speciation in aerosol dust influences iron bioavailability over glacial-interglacial timescales, *Geophysical Research Letters*, 40, 1618–1623, <https://doi.org/10.1002/grl.50296>, 2013.

Spott, O., Russow, R., and Stange, C. F.: Formation of hybrid N₂O and hybrid N₂ due to codenitrification: First review of a barely considered process of microbially mediated N-nitrosation, *Soil Biology and Biochemistry*, 43, 1995–2011, <https://doi.org/10.1016/j.soilbio.2011.06.014>, 2011.

910 Stauffer, B., Flückiger, J., Monnin, E., Nakazawa, T., and Aoki, S.: Discussion of the reliability of CO₂, CH₄ and N₂O records from polar ice cores, *Mem. Natl Inst. Polar Res.*, 139–152, 2003.

Su, Q., Domingo-Félez, C., Jensen, M. M., and Smets, B. F.: Abiotic Nitrous Oxide (N₂O) Production Is Strongly pH Dependent, but Contributes Little to Overall N₂O Emissions in Biological Nitrogen Removal Systems, *Environ. Sci. Technol.*, 53, 3508–3516, <https://doi.org/10.1021/acs.est.8b06193>, 2019.

915 Sutka, R. L., Ostrom, N. E., Ostrom, P. H., Gandhi, H., and Breznak, J. A.: Nitrogen isotopomer site preference of N₂O produced by *Nitrosomonas europaea* and *Methylococcus capsulatus* Bath, *Rapid Comm Mass Spectrometry*, 17, 738–745, <https://doi.org/10.1002/rcm.968>, 2003.

Sutka, R. L., Ostrom, N. E., Ostrom, P. H., Breznak, J. A., Gandhi, H., Pitt, A. J., and Li, F.: Distinguishing Nitrous Oxide Production from Nitrification and Denitrification on the Basis of Isotopomer Abundances, *Appl Environ Microbiol*, 72, 638–644, <https://doi.org/10.1128/AEM.72.1.638-644.2006>, 2006.

Tarasov, L. and Peltier, W. R.: Greenland glacial history, borehole constraints, and Eemian extent, *J. Geophys. Res.*, 108, 2001JB001731, <https://doi.org/10.1029/2001JB001731>, 2003.

920 Tian, H., Xu, R., Canadell, J. G., Thompson, R. L., Winiwarter, W., Suntharalingam, P., Davidson, E. A., Ciais, P., Jackson, R. B., Janssens-Maenhout, G., Prather, M. J., Regnier, P., Pan, N., Pan, S., Peters, G. P., Shi, H., Tubiello, F. N., Zaehle, S., Zhou, F., Arneth, A., Battaglia, G., Berthet, S., Bopp, L., Bouwman, A. F., Buitenhuis, E. T., Chang, J., Chipperfield, M. P., Dangal, S. R. S., Dlugokencky, E., Elkins, J. W., Eyre, B. D., Fu, B., Hall, B., Ito, A., Joos, F., Krummel, P. B., Landolfi, A., Laruelle, G. G., Lauerwald, R., Li, W., Lienert, S., Maavara, T., MacLeod, M., Millet, D. B., Olin, S., Patra, P. K., Prinn, R.



G., Raymond, P. A., Ruiz, D. J., van der Werf, G. R., Vuichard, N., Wang, J., Weiss, R. F., Wells, K. C., Wilson, C., Yang, 930 J., and Yao, Y.: A comprehensive quantification of global nitrous oxide sources and sinks, *Nature*, 586, 248–256, <https://doi.org/10.1038/s41586-020-2780-0>, 2020.

Tischer, J., Zopfi, J., Frey, C., Magyar, P. M., Brand, A., Oswald, K., Jegge, C., Frame, C. H., Miracle, M. R., Sòria-Perpinyà, X., Vicente, E., and Lehmann, M. F.: Isotopic signatures of biotic and abiotic N_2O production and consumption in the water column of meromictic, ferruginous Lake La Cruz (Spain), *Limnology & Oceanography*, 67, 1760–1775, 935 <https://doi.org/10.1002/lno.12165>, 2022.

Toyoda, S., Yoshida, N., Miwa, T., Matsui, Y., Yamagishi, H., Tsunogai, U., Nojiri, Y., and Tsurushima, N.: Production mechanism and global budget of N_2O inferred from its isotopomers in the western North Pacific, *Geophysical Research Letters*, 29, <https://doi.org/10.1029/2001GL014311>, 2002.

Toyoda, S., Mutobe, H., Yamagishi, H., Yoshida, N., and Tanji, Y.: Fractionation of N_2O isotopomers during production by 940 denitrifier, *Soil Biology and Biochemistry*, 37, 1535–1545, <https://doi.org/10.1016/j.soilbio.2005.01.009>, 2005.

Toyoda, S., Yoshida, N., and Koba, K.: Isotopocule analysis of biologically produced nitrous oxide in various environments, *Mass Spectrometry Reviews*, 36, 135–160, <https://doi.org/10.1002/mas.21459>, 2017.

Wilhelms, F., Sheldon, S. G., Hamann, I., and Kipfstuhl, S.: Implications for and findings from deep ice core drillings an 945 example: The ultimate tensile strength of ice at high strain rates, *Physics and Chemistry of Ice (The proceedings of the International Conference on the Physics and Chemistry of Ice held at Bremerhaven, Germany on 23-28 July 2006) The Royal Society of Chemistry Special Publication No. 311*, 635–639, 2007.

Wolff, E. W., Moore, J. C., Clausen, H. B., and Hammer, C. U.: Climatic implications of background acidity and other chemistry derived from electrical studies of the Greenland Ice Core Project ice core, *J. Geophys. Res.*, 102, 26325–26332, <https://doi.org/10.1029/96JC02223>, 1997.

950 Wrage-Mönnig, N., Horn, M. A., Well, R., Müller, C., Velthof, G., and Oenema, O.: The role of nitrifier denitrification in the production of nitrous oxide revisited, *Soil Biology and Biochemistry*, 123, A3–A16, <https://doi.org/10.1016/j.soilbio.2018.03.020>, 2018.

York, D., Evensen, N. M., Martínez, M. L., and De Basabe Delgado, J.: Unified equations for the slope, intercept, and standard errors of the best straight line, *American Journal of Physics*, 72, 367–375, <https://doi.org/10.1119/1.1632486>, 2004.

955 Zhu-Barker, X., Cavazos, A. R., Ostrom, N. E., Horwath, W. R., and Glass, J. B.: The importance of abiotic reactions for nitrous oxide production, *Biogeochemistry*, 126, 251–267, <https://doi.org/10.1007/s10533-015-0166-4>, 2015.